TÉCNICO LISBOA

Flashback and Blowoff Stability Analysis of Hydrogen Enriched Natural Gas using Bunsen Flames

Diogo Filipe de Deus Vozone

Thesis to obtain the Master of Science Degree in

Mechanical Engineering

Supervisor: Prof. Edgar Caetano Fernandes

Examination Committee

Chairperson: Prof. José Manuel da Silva Chaves Ribeiro Pereira

Supervisor: Prof. Edgar Caetano Fernandes

Member of the Committee: Prof. Teodoro José Pereira Trindade

October 2021

Acknowledgments

Esta tese representa a conclusão dos últimos meses de trabalho mas também o fim do curso no Instituto Superior Técnico. Foi um longo percurso e para o fazer tive muita ajuda, a qual agradeço:

Ao meu orientador Prof. Edgar Fernandes, pela confiança, ajuda e compreensão ao longo destes meses, e por me ter levado para a área de Energia pelo impacto que as aulas que leciona tiveram.

À Dr. Sandra Dias, ao Miguel Santos, Bruno Gouveia e Diogo Almeida, pela ajuda presencial no laboratório, fulcral para arrancar com os trabalhos experimentais.

Aos colegas e amigos Gonçalo Cunha, Miguel Silva, José Mota, Vasco Centeno e Miguel Borges, que me acompanharam durante o curso, em longos fins-de-semana, projetos, noites longas e também nos momentos de descanso e diversão.

Aos amigos que conheci em Ljubljana, Gomes, Joana, Inês e Mariana (and the foreign ones) e que tornaram esses meses numa das melhores experiências destes anos.

A toda a minha família e restantes amigos que não menciono aqui mas que não esqueço.

À minha mãe, ao meu pai e à minha irmã por me ajudarem no dia-a-dia de um longo trabalho como estes e oferecerem as melhores condições para que o pudesse fazer.

Um especial obrigado à Maria Inês por me ter acompanhado nestes meses e me ter ajudado nos momentos mais difíceis.

This work was developed at the Thermofluids, Combustion and Energy Systems laboratory of the IN+ - Center for Innovation, Technology and Policy Research.

Resumo

Nesta tese foram estudados os impactos do enriquecimento de gás natural com hidrogénio em aspectos fundamentais da combustão, como os fenómenos de flashback e blowoff em chamas de Bunsen. Análise dimensional foi usada para prever o início do flashback e também foram aplicadas técnicas de *particle image velocimetry* no escoamneto isotérmico para verificar se as suposições subjacentes normalmente feitas no estudo de gradientes de velocidade crítica eram válidas.

Seis misturas de combustível desde metano puro, NG100, a NG60 H40, 3 diâmetros diferentes, 7 mm, 10 mm e 14 mm e 6 diferentes razões de equivalência de 0,8 a 1,3, foram usadas nas experiências.

Duas equações que descrevem a variação dos gradientes de velocidade crítica para o gás natural com percentagem de hidrogénio xH_2 e razão de equivalência ϕ foram sugeridas. Relativamente aos limites de funcionamento de um queimador de Bunsen, os diâmetros e gamas óptimos de caudais admissíveis foram apresentados na forma de diagramas de Glassman e analisados para os teores de hidrogénio mais elevados aceites em Portugal tendo em conta o Índice de Wobbe.

A análise dimensional mostrou bons resultados ao interpolar os dados de flashback, fornecendo evidências de que "K" não é de facto constante, mas varia significativamente com as diferentes misturas utilizadas. Tomando os valores de K obtidos, a mistura NG90 H10 seria a menos suscetível a sofrer flashback enquanto a mistura NG60 H40 seria a mais suscetível a sofrer flashback. A comparação dos perfis de velocidade medidos com os perfis de velocidade calculados mostrou que a suposição de escoamento de Poiseuille pode fornecer valores não realistas ao calcular gradientes de velocidade crítica de blowoff.

Palavras-chave: flashback, blowoff, chama de Bunsen, hidrogénio, gás natural

Abstract

In this thesis, the impacts of hydrogen enrichment of natural gas in fundamentals combustion aspects such as the flashback and blowoff phenomena in Bunsen Flames were studied. At the same time, dimensional analysis was used to predict the onset of flame flashback and also applied particle image velocimetry techniques on the isothermal flow field to verify whether the underlying assumptions typically made on the study of critical velocity gradients were valid.

Six fuel mixtures from pure methane, NG100, to NG60 H40, 3 different diameters, 7mm, 10mm and 14mm and 6 different equivalence ratios from 0.8 to 1.3, were used in the experiments.

Two equations describing the variation of the critical velocity gradients for natural gas with hydrogen percentage xH_2 and equivalence ratio ϕ were suggested. Regarding the operation limits of a Bunsen burner, the optimum diameters and ranges of admissible flows were presented in the form of Glassman diagrams and analysed for with highest hydrogen content accepted in Portugal taking into account the Wobbe Index.

The dimensional analysis showed good results when interpolating the results of flashback data, providing evidence that "K" is not in fact a constant, but varies significantly with different mixtures used. Taking the values of K obtained, the mixture NG90 H10 would be the least susceptible to flashback while the mixture NG60 H40 would be the most susceptible to flashback. The measured velocity profiles comparison against the calculated velocity profiles showed that the assumption of Poiseuille flow can provide non realistic values when calculating blowoff critical velocity gradients.

Keywords: flashback, blowoff, Bunsen flame, hydrogen, natural gas

Contents

List of Tables

List of Figures

Nomenclature

Acronyms

DGEG	Direção Geral de Energia e Geologia
GUI	Graphical User Interface
HENG	Hydrogen Enriched Natural Gas
HHV	Higher Heating Value
IA	Interrogation Area
LHV	Lower Heating Value
LPM	Liters Per Minute
NG	Natural Gas
PIV	Particle Image Velocimetry
PVC	Polyvinyl Chloride
SG	Specific Gravity
SLPM	Standard Liters Per Minute
WI	Wobbe Index

Symbols

λ	Thermal conductivity
μ	Dynamic viscosity
ϕ	Equivalence ratio
ρ	Density
τ_f	Characteristic time scale of the flow
τ_P	Response time of the flow
c_p	Specific heat at constant pressure

d	Diameter
d_p	Penetration distance
g_B	Critical blowoff gradient
g_F	Critical flashback gradient
Pe_F	Péclet Number based on laminar burning velocity
Pe_J	Péclet Number based on jet velocity
S_L	Laminar burning velocity
Stk	Stokes Number
u_{av}	Average stream velocity
v	Kinematic viscosity
xH_2	Volumetric percentage of Hydrogen in the mixture
Da	Damköhler Number
Q	Volumetric flow rate
R,r	Radius
Re	Reynolds Number

Chapter 1

Introduction

1.1 Motivation

As the third decade of the XXI century unrolls and one hundred and eighty years have passed since the end of the industrial revolution, the consequences of irresponsible usage of fossil fuels, over-consumption and neglecting the environment are present in our day-to-day more than ever.

The growing global conscience and technological advances (from artificial intelligence to carbon nanotubes), make it possible to tackle consequences such as climate change, global warming, air pollution and fossil fuel dependency.

Climate change is one of the main causes for global concern, reflected in the rise of global temperature, extreme weather events, drought, biodiversity and more. Eighty to ninety percent of natural disasters in the last 10 years are due to floods, droughts and severe storms and two hundred and fifty thousand additional deaths are expected to happen from climate-sensitive diseases from 2030 onward [1].

Adding to these global challenges, local ones also need to be addressed such as individual countries energetic and fossil fuel dependency. According to *Direção Geral de Energia e Geologia*, Portugal's energy dependence in 2017 was 79,7% [2]. Both energetic and economic dependencies on other countries are undesirable characteristics of a country's economy and, at a country level, changes must be made to reduce these dependencies.

Engineering and science in general play a big role on overcoming these hard challenges. Particularly, the study of mechanical engineering and combustion has the possibility of changing the next decades' path towards a greener and more sustainable society. It is of the utmost importance to come up with viable solutions that are compatible with this decade's demands without compromising the current standards of living.

Hydrogen can be a key part in the complex energy system worldwide and specifically, in Portugal. Therefore, this thesis aims to improve the knowledge around the topic and complement the existing literature on hydrogen enrichment of natural gas and its potential in Portugal in the upcoming years.

1.2 Energy Transition and Hydrogen's role in the future energy system

In order to face the current global challenges relating climate change, global warming and greenhouse gases emissions, a big effort has been put in place in the last decades by governments, non-governmental organisations, industries and scientists towards a more sustainable, healthy and green presence for future generations.

As a result of this effort, the technologies involving renewable electricity generation are growing fast and alternative sources of energy are being developed across multiple sectors to take advantage of the low cost, high security and many health benefits that come with it.

Hydrogen can be seen as an energy intermediate in the future energy system, connecting different industries and covering a wide range of usages through its life-cycle.

"Hydrogen at Scale concept" [3], represented in the schematics of Figure 1.1, proposes hydrogen as a third energy infrastructure, joining the electric grid and the natural gas infrastructure. On the generation side, hydrogen can be produced using various conventional and renewable energy sources. On the application side, hydrogen has many current and possible future applications across the sectors of transportation, chemical and industrial processes, fertilisers and heat production.

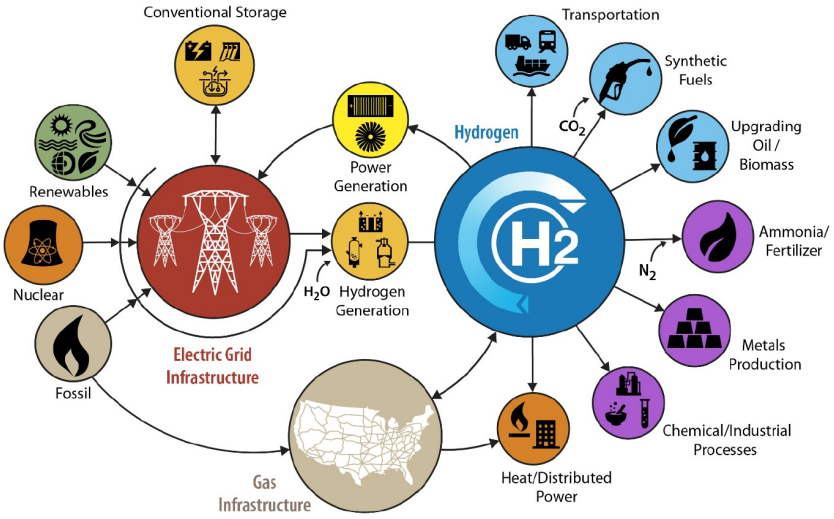

Figure 1.1: Schematic illustration of the "Hydrogen at Scale" concept [3].

In fact, the European Hydrogen Strategy, launched by the European Commission, aims to install a capacity of 40 GW of green hydrogen production until 2030, contributing to make Europe the first carbon neutral continent. Also, the share of hydrogen in Europe's energy mix is projected to grow from the current less than 2% to 13-14% by 2050 [4].

In the Portuguese context there are also goals and objectives regarding the implementation of green hydrogen in the country. The following goals have been set to attain by the year 2030: injection of 10%-15% of H_2 in the natural gas network, 2%-5% H_2 in the industry consumption as also projects to increase the production capacity of green hydrogen to a total of around 2.5 GW [5].

1.3 Combustion of Premixed Flames

1.3.1 Flame Phenomena and Flame Structure

Since premixed Bunsen-burner flames will be the center focus of this thesis, it is important to start by addressing the basic concepts involved such as the flame structure, laminar flame speed and what factors influence it.

A basic definition of what a flame is is offered by Stephen R. Turns' work in which is mentioned that "a flame is a self-sustaining propagation of a localised combustion zone at subsonic velocities" [6]. To specify, Bunsen burners are used to obtain laminar premixed flames, which main characteristics are a relatively high temperature, a blue flame with low radiation and no soot emissions.

Many household, commercial, and industrial equipment and processes use laminar premixed flames, which are often used in conjunction with diffusion flames. Gas stoves and ovens, as well as heating appliances and Bunsen burners, are examples. Laminar, premixed natural-gas flames are also commonly used in the production process of glass products, for example.

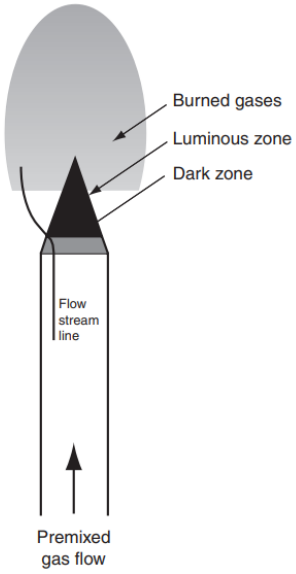

Figure 1.2: Schematic illustration of a Bunsen burner and the flame it produces [7].

Figure 1.2 shows a schematic illustration a of Bunsen burner which typically is a circular tube into which a combustible mixture is introduced. This mixture is ignited at the open end of the tube and the resultant flame takes the shape of a nearly conical surface [8]. As illustrated, this type of flames has two zones: a fuel-rich premixed inner flame, surrounded by a diffusion flame [6]. The secondary reaction zone results when the carbon monoxide and hydrogen products from the inner flame encounter the ambient air.

The laminar flame speed is an important parameter of a combustible mixture. The value of the flame speed has important effects upon the propensity of the flame to flashback and blowoff, and it also controls other key combustion characteristics, such as the flame's spatial distribution [9].

The shape of the flame obtained is typically conical due to the effects of the velocity profile and heat

losses to the tube wall. For the flame to remain stationary, the flame speed must equal the speed of the normal component of the unburnt gas velocity. This principal is shown mathematically by Eq. 1.1 below [6] for the laminar flame speed S_L in which v_u is the velocity of the unburnt gases and α is the angle between the tube's axis and the inner flame front.

$$S_L = v_u \sin \alpha \tag{1.1}$$

Some of the factors influencing flame speed are the temperature of the reactants, equivalence ratio, pressure, flame curvature and flame temperature. The temperature of the reactants was a special concern in this work since other authors such as Lewis and Von Elbe and students previously working in similar setups in this laboratory reported high tube temperatures that would definitely impact the downstream flow, and consequently the flame speed. This concern will be addressed later in the thesis, explaining the cooling system designed for the setup.

Experimental data for hydrocarbon flames burning in air show that the laminar flame speed changes with the temperature of the reactants according to:

$$S_L \propto T_o^m \tag{1.2}$$

with m ranging between 1.5 and 2.0, and a specific example of stoichiometric flames of methane/air can be calculated using the following empirical correlation [10]:

$$S_L(\text{cm/s}) = 10 + 3.71 \times 10^{-4} T_o^2 \tag{1.3}$$

Equivalence ratio is another factor influencing the burning velocity of flames. It can be defined as the ratio of the fuel mass flow rate to the air mass flow rate divided by the same ratio at the stoichiometry of the reaction considered [11].

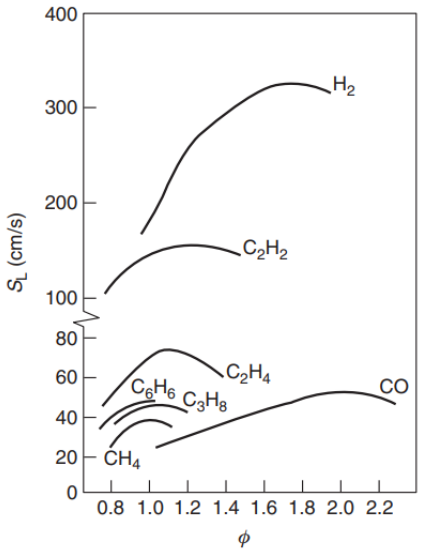

Figure 1.3: Variation in laminar flame speeds with equivalence ratio for various fuel–air systems at 1 atm and 298K. [7]

Given the fact that the adiabatic flame temperature is a function of the equivalence ratio and since the maximum adiabatic flame temperature, in the case of hydrocarbons, reaches a maximum at $\phi = 1$ or slightly higher than 1, the same happens with the burning velocity. This variation in laminar flame speeds is presented in the plot of Fig. 1.3.

The peak of S_L shifts to $\phi = 1.8$ for hydrogen due to the substantial increase of the thermal diffusivity with equivalence ratio ϕ. At a temperature of T = 298 K and pressure P = 1 atm, the values for the laminar flame speed of hydrogen (H_2), methane (CH_4) and propane (C_3H_8) are 219.7 cm/s, 36.2 cm/s and 46.3 cm/s, respectively [7]. Hydrogen has a higher laminar flame speed than the hydrocarbons due its higher thermal diffusivity.

The other two important flame phenomena to introduce are the phenomena of flame flashback and flame blowoff and these are both related to equilibrium between the mass flow rate of the mixture and the local burning velocity.

If the velocity of the mixture exceeds the laminar flame speed, the flame front will move in the same direction as the mixture, towards the burner exit. The other way around, if the laminar flame speed exceeds the velocity of the mixture, the flame will propagate upstream into the tube, which could potentiate security problems.

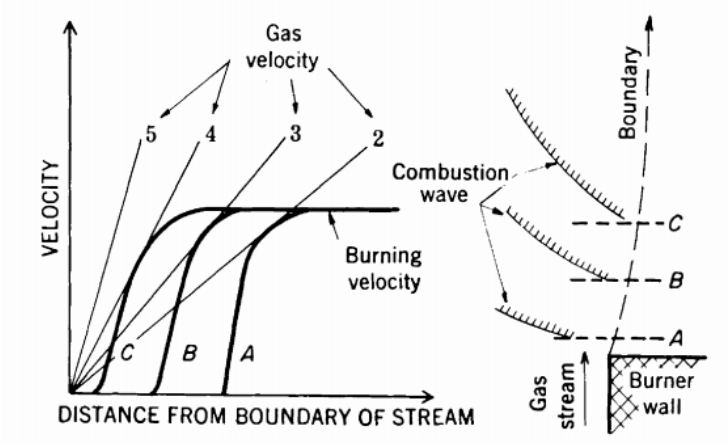

Figure 1.4: Schematic illustration of flashback and blowoff [12].

Both phenomena are represented schematically in Fig. 1.4 where on the right are three possible stable flame positions A, B and C. These, in turn, equate to a burning velocity curve A, B and C on the left. Curves 2, 3, 4 and 5 represent the linear approximation of different gas velocities.

Curve 2 is tangent to the burning velocity curve and therefore defines the upper limit of gas flow at which flashback occurs. As the gas velocity increases, the burning velocity curve progressively moves toward the boundary until a critical gas velocity curve 4 is reached which is the blowoff limit. On further increase (curve 5) the gas velocity exceeds the burning velocity everywhere, and the flame blows off. The critical velocity gradients g_F and g_B are given by the slopes of curves 2 and 4, respectively. The concept of critical velocity gradients will be further analysed in Section 1.4.

1.3.2 Interchangeability of Gaseous Fuels

When considering injecting any gas into an existing gas appliance or system, is is mandatory that the replacement gas is able to deliver energy at a sufficiently high rate. To take into consideration the calorific content of the gas, both the Higher Heating Value, HHV, defined as the energy released per unit mass when all combustion products are cooled down, and the Lower Heating Value, LHV, which assumes that the combustion products remain at a high temperature without vapour condensation, can be used as measurements to compare different fuels.

However, interchangeability was an important issue in the beginning of the natural gas business, since in most places natural gas was introduced as a replacement for manufactured gas. At this time, the Wobbe Index, WI, became the standard measurement of interchangeability between gaseous fuels. Regardless of calorific value, gases with the same WI produce the same heat load in a gas burner. Therefore WI is by far the most important combustion parameter for gas appliances. [13].

The Wobbe Index [MJ/Nm^3] is normally defined as [14]:

$$WI = \frac{HHV}{\sqrt{SG}} \tag{1.4}$$

where HHV [MJ/Nm^3] is the higher heating value, and SG is the specific density of the gas compared to air, dimensionless.

Wobbe Index values for natural gas vary according to its specific composition, but a value of 51 MJ.Nm^{-3} may be taken as a characteristic lower bound for natural gas supplied with several European countries [15], while a value of WI = 48.6 MJ.Nm^{-3} may be assumed for hydrogen. In the scope of this work it is interesting to analyse how the index varies with the addition of hydrogen to natural gas, and this is the information shown in Fig. 1.5.

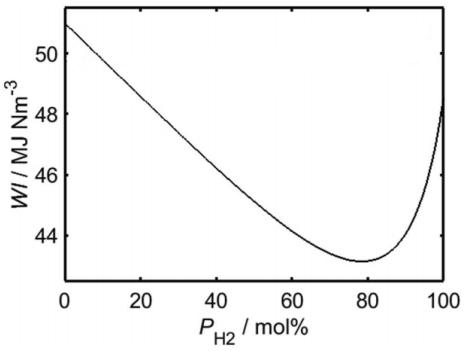

Figure 1.5: Variation of the Wobbe Index as a function of molar hydrogen percentage in HENG. Adapted from [15]

With the graph above in mind, it is interesting to note that nowadays, in Portugal, the range of accepted values of Wobbe Index by national regulation is between 49.43 MJ.Nm^{-3} and 52.76 MJ.Nm^{-3} [16], which does not seem to permit percentages of hydrogen any higher than 20%, strictly looking into the Wobbe Index information.

1.3.3 Stability limits of laminar flames and burner design

The operational conditions and design of home cooking stoves are very similar to those in Bunsen tubes. In the design of a Bunsen burner, it is desirable to have the maximum range of volumetric flow without encountering stability problems.

The analysis of these ranges of volumetric flows is facilitated with the use of "Glassman diagrams", that when following a set of basic conditions will provide the safest operational area for a Bunsen tube using a specific fuel. Figure 1.6 below shows this exact diagram, and the respective set of "boundary" equations [7].

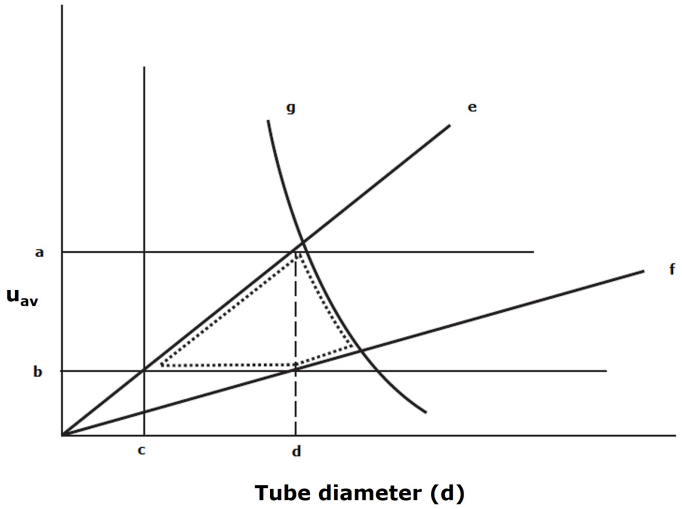

Figure 1.6: Caption for figure.

- Equation a): $u_{av} = 5S_{\mathrm{L}}$. If the average velocity is higher than 5 times S_{L}, the fuel penetrates the Bunsen cone tip and "yellow tips" appear.
- Equation b): $u_{av} = 2S_{\mathrm{L}}$. The average velocity must be at least twice S_{L} for a precise Bunsen cone to form.
- Equation c): $d = 2d_{\mathrm{p}}$. The diameter d must be at least twice the penetration distance: greater than the quenching distance, otherwise a precise Bunsen cone will not form.
- Equation e) and f): $u_{\mathrm{av}} = \frac{g_{\mathrm{B}}}{8}d$, $u_{\mathrm{av}} = \frac{g_{\mathrm{F}}}{8}d$. These equations take into account the instabilities caused when blowoff and flashback limits are reached.
- Equation g): $Re = \frac{u_{\mathrm{av}}d}{v} = 2000$. If the Reynolds number of the combustible gases in the tube exceeds 2000, the flow can become turbulent, destroying the laminar characteristics of the flame.

When all these requirements suggested by Glassman [7] are met, the dashed area will provide the "safe zone" of operation for the specific fuel in use. An optimal diameter can also be chosen, in the diagram marked with the letter "d", which will provide the biggest variability of flow velocities without encountering stability issues. This diameter has a typical value around 10mm for a Bunsen tube.

1.4 State of the Art

In 1943, Bernard Lewis and Guenther von Elbe publish the work "Stability and Structure of Burner Flames" [12] in which it is proposed the concept of critical velocity gradient g_c. This work meant to remedy the omission by previous theories of explanations for the exact conditions in which flashback and blowoff occur.

This velocity gradient concept is traditionally used to describe the phenomena of blowoff and flashback and is based on the laminar jet flame's tendency to propagate upstream or downstream when the laminar burning velocity exceeds or subceeds the local flow velocity. It is also mentioned by Lewis and von Elbe that the critical velocity gradient for flashback "is obviously determined solely by factors that affect the burning velocity near the wall, namely, the condition of the wall (temperature mainly) and the mixture composition".

The proposed gradient,

$$g_{\mathrm{F,B}} \equiv -\lim_{r \to R}(du/dr) \tag{1.5}$$

is explored for different natural gas-air mixtures and tube diameters. The authors also report that the results are affected by the increase in tube temperatures up to about 100 $^{\mathrm{o}}$C, in glass tubes. This concern is addressed later in this thesis and is achieved by cooling of the burner tubes used.

Later, in 1948, Abbott Putnam and Randolph Jensen, based on the work of Lewis and von Elbe, publish a work [17] in which a dimensionless approach is taken to attempt to obtain a more general interpretation of flashback and blowoff.

As an explanation of the flame-holding mechanism, Lewis and von Elbe [12] have presented a velocity gradient concept which permits a qualitative interpretation of the data concerning stability analysis. It is, however, an analysis tool which is limited to the operational conditions and gas compositions used at each experiments. With this in mind, different dimensionless approaches have been suggested, including using "Damköhler numbers" Da (ratio of reaction timescale to the convection time scale) as a flashback propensity indicator and using "Peclet numbers" Pe. The latter is the approach suggested by Putnam and Jensen [17].

Putman and Jensen proposed that the onset of flashback may be defined by the "Peclet numbers" Pe_F (flame Peclet number) and Pe_J (jet Peclet number):

$$Pe_F = \frac{2RS_L c_p \rho}{\lambda} \tag{1.6}$$

$$Pe_J = \frac{2Ru_{av} c_p \rho}{\lambda} \tag{1.7}$$

where R is the tube radius, S_L is the laminar flame speed, c_p the specific heat at constant pressure, ρ the density, λ the coefficient of thermal conductivity and u_{av} is the average jet velocity.

The authors suggested that the flashback propensity of a given fuel could be approximated using the relationship between the two "Peclet numbers":

$$Pe_J = \frac{1}{8K}(Pe_F)^2 \tag{1.8}$$

where K is a fuel-dependent constant in the order of magnitude of 1 and the final approximation holds when K/P_F is much less than one.

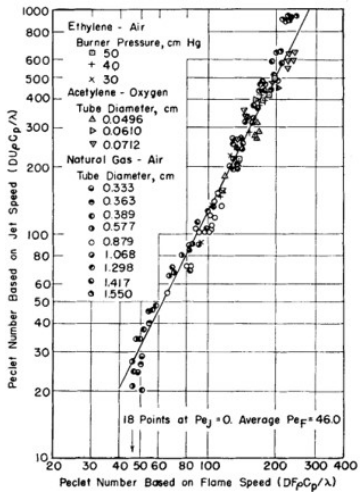

Figure 1.7: Representation of flashback data on ethylene-air, acetylene-oxygen, and natural gas-air [17]

Figure 1.7 shows the application of the suggested relationship on data regarding natural gas-air mixtures for several sizes of burners superimposed on ethylene-air mixtures at various burner pressures and acetylene-oxygen in various tube sizes. The data fall into a pattern predicted by the theoretical considerations.

It is also included in this publication a discussion by another author, Kurt Wohl, where he mentions that it does not seem to be permissible to treat "K" as a constant. This idea will be further analysed in Chapter 3.

In a more recent work, 2015, Duan and McDonell [18] selected the critical Damköhler number as the indicator of flashback propensity. The authors developed an empirical physical model for flashback propensity as a function of dimensionless groups.

The potential variables determining flashback behaviour where catalogued into five types: operational parameters, unburnt conditions, ambient conditions, rig properties, and others. An extensive list of parameters determining flashback behaviour is presented and another list with the respective relations among the listed parameters. Furthermore, the Buckingham Pi theorem was used to conduct a dimensional analysis that resulted in the following expression for the critical Damköhler number [18]:

$$Da = \text{ Const. } \cdot Le^{-6.12} \cdot \left(\frac{T_u}{T_0}\right)^{-1.71} \cdot \left(\frac{T_{tip}}{T_u}\right)^{-3.69} Pe_f^{1.89} \cdot f_1\left(\frac{\theta'}{d}\right) \cdot f_2\left(\frac{P_u}{P_0}\right) \tag{1.9}$$

This model suggests a concrete significance of various parameters such as preferential diffusion (Le), heat loss ($\frac{T_u}{T_0}$), thermal coupling effect ($\frac{T_{tip}}{T_u}$) and flame Péclet number (Pe_f). Higher Damköhler number Da values indicate less mass flow is required to avoid flashback, i.e. greater flashback resistance.

Duan and McDonell reported good correlation between the existing data and the resulting correlation,

providing reasonable ability predicting flashback tendencies for the parameters studied. An example of these correlations is shown in Fig. 1.8. This is despite mentioning that the studies on the subject generally emphasise laminar conditions while their work focused on turbulent conditions.

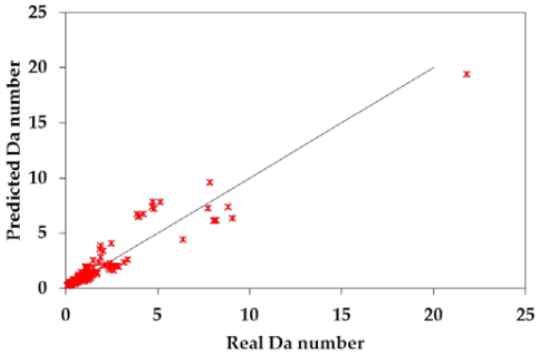

Figure 1.8: Comparison of the real and predicted Da values using Eq. 1.9 [18]

The work of Jones and Dunnill [15] focuses on the practical challenges ahead when considering the hydrogen enrichment of domestic natural gas in the United Kingdom. The physical properties of hydrogen make it impossible to simply interchange the two gases without a major overhaul of the existing energy network [15]. It is essential to ensure that neither flashback or blowoff could occur during a changeover from natural gas to HENG.

It is also imperative that the replacement gas is able to deliver energy at a sufficiently high rate. Employing Bernoulli's principle, a higher volume of HENG is admitted than natural gas during a given time period due to its lower density, which serves to counteract the reduction in carbon dioxide during a constant time procedure.

It has been shown by the authors that whilst hydrogen-enrichment acts to lower the calorific value of natural gas, it also augments the stability of a burner by suppressing the occurrence of flame blowoff and prevents yellow tipping by lowering the oxygen-requirements of the fuel.

It is also concluded that for ports less than 3.5mm in diameter, HENG fuel containing as much as 50 mol% hydrogen may be ignited safely without risk of flashback while flashback upon extinction of the flame occurs only if the hydrogen proportion exceeds approximately 34.7 mol%.

Jones and Dunnill end the work by mentioning that to properly evaluate the virtues and shortcomings of a given proposed composition of hydrogen-enriched natural gas, quantifying the physical effects of hydrogen-enrichment as a function of hydrogen percentage is a critical first step.

1.5 Scope of the Work

Given the motivation and introduction presented, with consideration to the high impact on the future energy system that the use of green hydrogen can have, specially applied to the existing natural gas system, and attempting to complement the existing literature on the subject, this thesis proposes to contribute with relevant experimental insight to the flashback and blowoff stability analysis using Bunsen flames.

In order to reach these goals, methane and hydrogen are used to create flames of a wide range of conditions, lean, stoichiometric and rich premixed flames. Six mixtures with different hydrogen percentages are used while experimenting with three different tube diameters.

The different techniques/methodologies to attain the goals established are described also in this thesis such as the setup for the stability experiments and the particle image velocimetry experiments to analyse the flow velocity profiles.

It is here intended to provide concrete information regarding flame stability limits (flashback and blowoff) on HENG mixtures and useful plots such as the Glassman diagrams to assist in the design of Bunsen burners or other similar burners.

Another key focus of this thesis is to perform a dimensional analysis of flashback propensity and contribute to whether or not a constant "K" can be treated as a constant as suggested by some authors or it is fuel dependent and can have an impact on flashback propensity, an important security aspect when considering, for example, the injection of hydrogen in the natural gas network in the near future.

Chapter 2

Experimental Work

2.1 Flame stability test

2.1.1 Laboratory Setup

The laboratory setup used for the stability tests has the goal of visualising the occurrence of both flame flashback and blowoff in a Bunsen burner, for a wide range of different mixtures and different tube diameters while maintaining sufficient cooling for the burner and guaranteeing safety measurements and the most similar conditions possible for the different tests.

This was achieved using a simple setup, represented graphically in Figure 2.1, of gas bottles (CH_4 and H_2) and compressed atmospheric air, connected through security valves and flow meters to a mixing chamber. These are connected to the Bunsen burners via a 3D printed adaptors. The metallic area of this set (tube plus adaptor) is cooled using a cooling sleeve designed for the purpose, which uses flowing water as a cooling liquid controlled also by a flow meter. All the flow meters are controlled by a GUI in LabView through a computer.

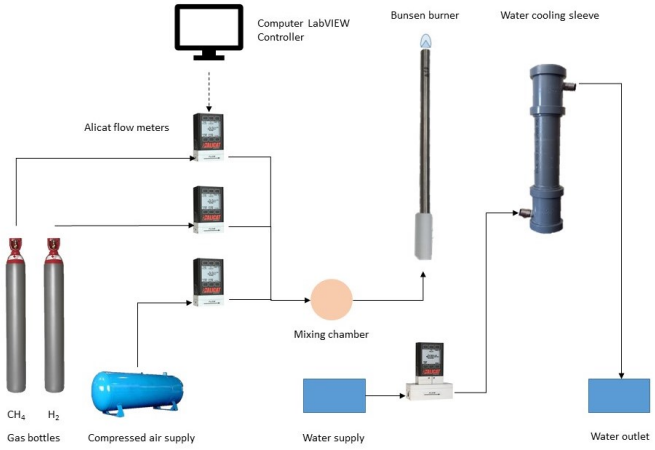

Figure 2.1: Diagram of the experimental setup used for the flame stability tests.

Equipment details

The gas flow meters used for the CH_4, H_2 and air are Alicant Scientific M-series high precision flow meters. Different arrangements of flow meters were used, taking always into consideration the minimum uncertainty possible, using the smallest flow meter capacity possible for each round of tests. Through all flashback and blowoff tests the following capacities of flow meters were used: 1 SLPM, 5 SLPM, 20 SLPM and 50 SLPM.

The unburnt and unmixed methane and hydrogen are stored in Air Liquid Alphagaz 99.95% gas bottles kept under high pressure. The air used is atmospheric air from the compressed air piping system installed in the laboratory and is filtered and dried before being fed to the flow meter and posteriorly the the mixing chamber.

The Bunsen tubes consisted of 3 Stainless Steel (ANSI 304) tubes with the diameters of 7 mm, 10 mm and 14 mm and a wall thickness of 1 mm. Each tube's length was chosen to guarantee that the flow was fully developed and the streamlines were as undisturbed as possible after the mixing chamber and the quenching net. Taking this into consideration, the tube lengths are at least twenty times the diameter of the respective tube: 140 mm (7 mm tube), 200 mm (10 mm tube) and 280 mm (14 mm tube).

In the areas connecting the adaptors and the Stainless Steel tubes, honeycomb shaped steel quenching nets were placed to prevent flame propagation upstream that could harm the equipment and create unsafe situations when flame flashback was induced, even though the mixture flow would be cut off as soon as that happened.

In order to improve the previously existing Bunsen burner setup, a water cooling sleeve was designed. To make it easily interchangeable between different Bunsen burner sizes (varying both in diameter and length) it is composed of a fixed bottom part and a fixed top part that have adaptors to the water input and output tubes and a middle part that varies in length according to the tube diameter to be tested. All the five parts (two fixed and three varying) are PVC (polyvinyl chloride), with internal diameter of 34 mm and connected to each other and to the Bunsen burners through leak-proof rubbers. The PVC was chosen due to it being easily manipulated (cut, drilled, sanded, etc.) with the available machinery on the laboratory, its resistance to internal and external corrosion and its good thermal insulation characteristics.

Water is fed to the cooling sleeve from the bottom connector and leaves through the top connector at atmospheric pressure. This bottom to top continuous water flow guarantees that all the tests are performed with the Bunsen burners cooled at approximately the same distance from their top, around 10 mm, and that the temperature of the water remains low enough to provide a quick cooling effect.

2.1.2 Methodologies

Data acquisition

The data points regarding the flame stability experiments were obtained directly through the Bunsen tubes setup. The tests performed consisted in inducing both flashback and blowoff to a stable flame. This was achieved, in the former, through a consistent decrease in flow rate (small steps of Re), while keeping the composition constant, until the flame is unable to stabilise itself and enters the tube. The same approach was taken to blowoff tests, using Re changes in the opposite direction, i.e. through a consistent increase in the mixture flow rate until the flame is lifted and "leaves" the Bunsen tube.

Before proceeding with the presented experiments, a round of "control tests" was performed in order to obtain validation of the setup and methods used. This was done performing blowoff and flashback stability tests for pure methane (CH_4) without any H_2 addition and comparing the results with data from tests performed previously by another student using the same mixture and setup. The results were very satisfactory, thus validating the approach taken. The differences encountered were explained by the usage of the cooling sleeve that makes the data more reliable, specially in the flashback tests were a increase in the tube's temperature is noticeable and influences the thermodynamic interactions near the tip of the tube.

A first graph was plotted for each experiment during data acquisition for validation of the expected trends, plotting each Re that achieved instability versus ϕ, as it is shown as an example in Figure 2.2. Accounting for both flashback and blowoff tests, the total number of stability data points acquired were 189.

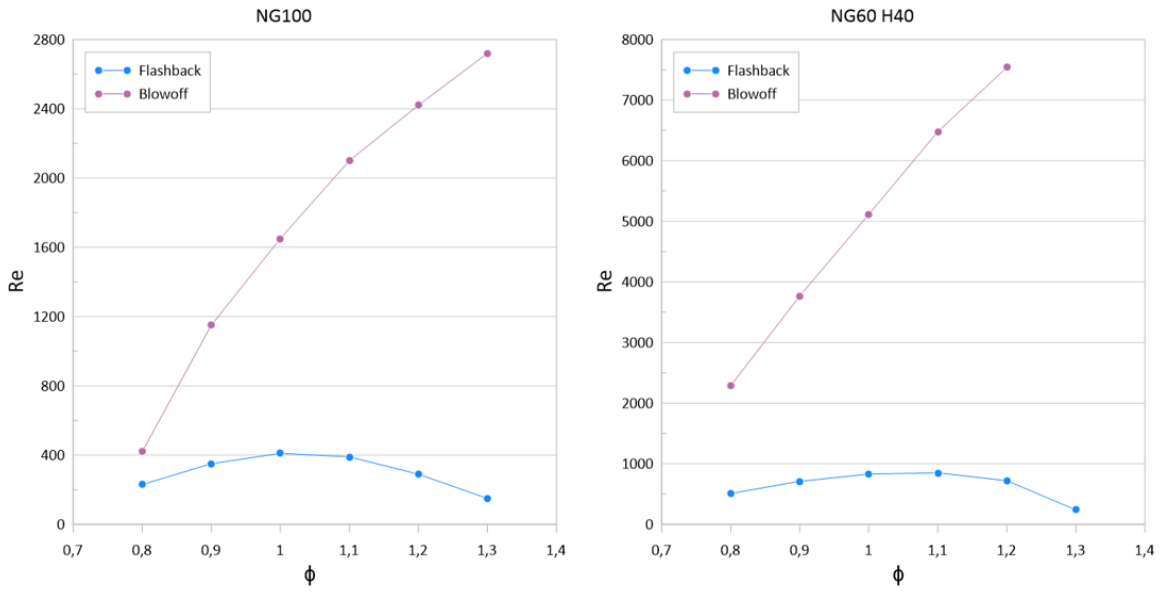

Figure 2.2: Flame stability tests for NG100 and NG60 H40 (d=10mm).

In order to obtain quantitative stability measurements between different mixture compositions and mixture equivalence ratios and compare the respective stability regions (using Glassman diagrams) the data points taken from the laboratory experiments were processed.

To follow the Glassman's diagram methodology presented in [7], "critical velocity gradients" for flashback and blowoff must be calculated. This gradient is defined as:

$$g_{\mathrm{F,B}} \equiv -\lim_{r \to R}(du/dr) \tag{2.1}$$

Assuming the flow profile of the unburnt gases in the exit of the Bunsen tube is parabolic and that Poiseuille flow exists, the gas velocity along a streamline is given by:

$$u = n\left(R^2 - r^2\right) \tag{2.2}$$

where R is the tube radius. Since the volumetric flow rate, Q (m^3/s) is given by

$$Q = \int_0^R 2\pi r u dr \tag{2.3}$$

then n must be equal to:

$$n = 2Q/\pi R^4 \tag{2.4}$$

This means we can calculate $g_{\mathrm{F,B}}$ using equations 3.4, 2.2 and 2.4:

$$\frac{du}{dr} = \frac{d}{dr}\left[\frac{2Q}{\pi R^4}\left(R^2 - r^2\right)\right] = -\frac{4Qr}{\pi R^4} \tag{2.5}$$

$$g_{\mathrm{F,B}} \equiv -\lim_{r \to R}(-\frac{4Qr}{\pi R^4}) = -\frac{4Q}{\pi R^3} \tag{2.6}$$

Substituting $Q = u_{av}.\pi R^2$ as the volumetric flow rate, taking into account the average flow velocity of the experiments and the definition of Reynolds number, one obtains:

$$g_{\mathrm{F,B}} = \frac{8}{d}u_{av} = \frac{8\nu}{d^2}\mathrm{Re} \tag{2.7}$$

The values for *kinematic viscosity* ν were calculated through the relation $\nu = \mu/\rho$. In turn, these were obtained using Cantera Python algorithms [19] that compile information based on the kinetic mechanism GRI-Mech 3.0 [20].

As found in the literature, the wall velocity gradients should remain constant at flashback and blowoff conditions for various flow-rates and tube diameters [17].

This is confirmed by the approach shown in Fig. 2.3 were the values compared are now of the same mixtures and the three different tubes instead of the approach shown in Fig. 2.2 were we have a view with fixed diameter and variable mixtures. In this case it is shown as an example the results for NG 100 and the proximity between the values.

To obtain the singular values for the gradients $g_{\mathrm{F,B}}$ needed to compute the Glassman's diagram, an average of each three values (three diameters) was taken and the results for all mixtures are further shown in Chapter 3.

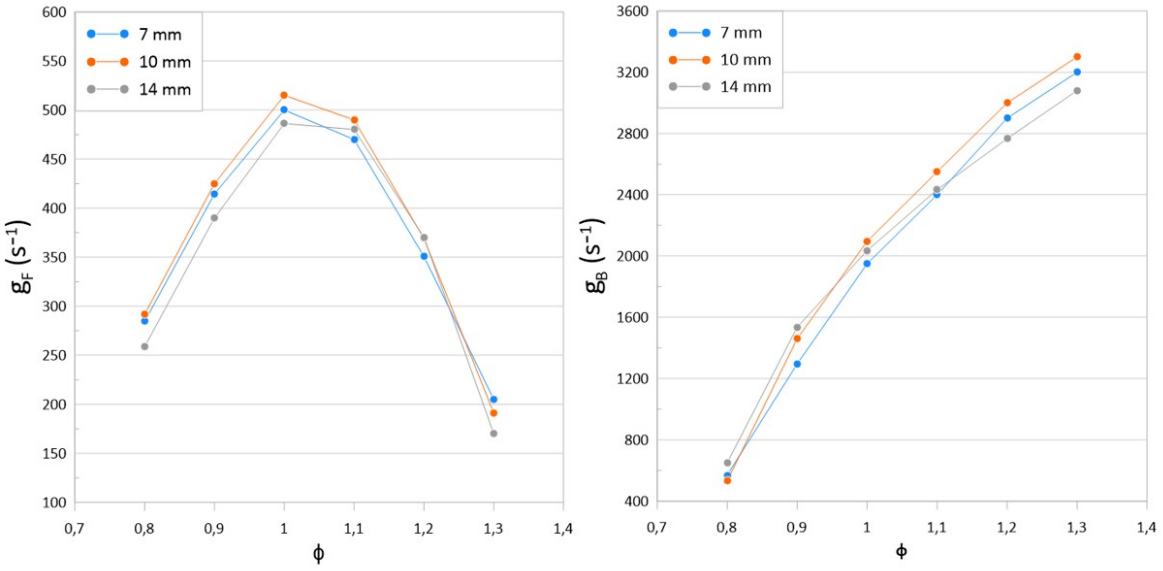

Figure 2.3: Velocity gradients at flashback (left) and blowoff (right) of NG 100 for tube diameters 7 mm, 10 mm and 14 mm.

2.2 Particle Image Velocimetry (PIV)

2.2.1 Laboratory setup

The laboratory setup for the Particle Image Velocimetry (PIV) tests is shown in the photograph of Fig. 2.4. It was assembled with the goal of obtaining cross sectional velocity profiles at the exit of the Bunsen burner tubes. This enables us to evaluate to some degree the suitability of the critical velocity gradients calculated using Eq. 3.1. This can be done comparing the real velocity profiles obtained via Particle Image Velocimetry and the "theoretical" profiles expected via the mentioned approach.

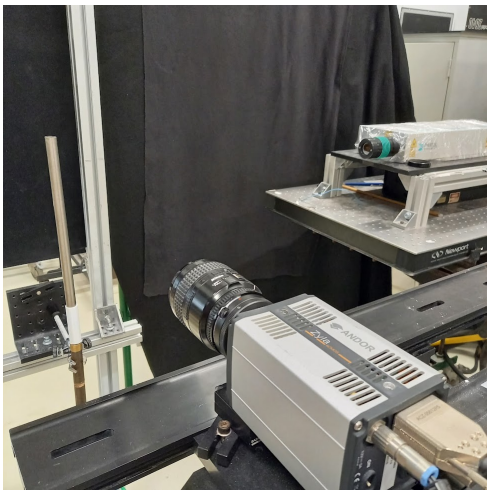

Figure 2.4: Experimental setup for the PIV experiments. Camera on the center, laser on the top right of the picture and Bunsen tube on the left.

The setup is composed of the same setup used in the flame stability tests presented in Section 2.1.1, without the water cooling sleeve and water supply, and additionally using a laser, camera, synchronizer, seeding flask with tracer particles and a magnetic stirrer.

Since a primary source of error when using tracer particles in PIV is the influence of gravitational forces on the velocity of the tracer particles, we must take into account fluid mechanical properties such as the particle Stokes number [21]:

$$\mathrm{Stk} = \frac{\tau_\mathrm{P}}{\tau_\mathrm{f}} \tag{2.8}$$

with the response time τ_P given by:

$$\tau_\mathrm{P} = d_\mathrm{p}^2 \frac{\rho_\mathrm{p}}{18\mu} \tag{2.9}$$

and τ_f standing for the characteristic time scale in the flow. In Eq.2.9, d_p is the particle diameter, ρ_p is the density of the particle and μ is the dynamic viscosity of the fluid.

It is suggested a value of Stokes number below 10^{-1} for an acceptable flow tracing accuracy. In this present case, aluminium oxide (Al_2O_3) particles were used with a density of 3950 kg/m^2 and a diameter of 1μm. The value of τ_f was inferred as a ratio between a length scale and a characteristic velocity of the flow. This resulted in a Stokes number of the order 10^{-3}.

The seeding flask is agitated to limit the probability of channel formation inside the fluidized bed [21] and to obtain a good particle density. It's enough to have a shaker motor attached to the seeding flask, in this case a magnetic stirrer with adjustable frequency.

The laser used to illuminate the tracer particles was a Dantec DualPower 65-15 Nd:YAG laser. It has a repetition rate between 0-15 Hz, a wavelength of 532nm and a beam diameter of 4mm.

To receive the light scattered by the tracer particles and capture the respective images, an Andor Zyla 5.5 sCMOS camera with a Nikon AF Nikor 60mm f/2.8D lenses were used in a direction perpendicular to the laser sheet.

Completion and synchronisation of the system were achieved using a synchronizer BNC Model 575.

Multiple laser and camera properties such as trigger rate, time between frames and number of frames were defined for each analysis using the software Dantec DynamicStudio [22].

2.2.2 Methodologies

A two phase approach was taken in the experiments to obtain the velocity profiles at the Bunsen tubes exits. These two phases are explained briefly in Fig. 2.5 and in more detail in the Results Section 3.4.

As described in the former, a first phase had the goal of creating a "baseline" to work with for the second phase. This means comparing in isothermal conditions (no flame) the velocity profiles obtained when the studied mixture was pure air with the velocity profiles obtained from experiments using only CH_4 (NG 100) and the natural gas mixture with the highest xH_2 (NG60 H40). If the profiles overlap sufficiently such that they could be interchangeable, for the second phase only air flow is necessary to simulate the results obtain with the other mixtures. For this comparison to be valid, all the other variables were kept fixed such as the Reynolds number and tube diameter.

The second phase consisted in using air as the fluid in study and selecting flow conditions that, if a combustible mixture were used with a flame, produce instability events such as flashback and blowoff, in all the diameters under study. The flow velocities, i.e. Reynolds numbers, were chosen taking into account the data from the flame stability tests to be representative of both the flashback and blowoff regions.

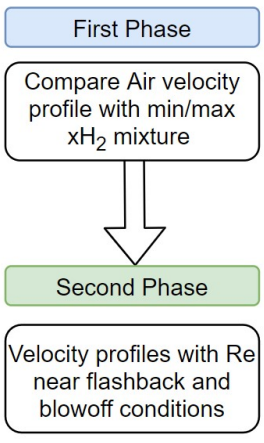

Baseline with Isothermal Laminar flow		
Air	Laminar flow	d = 10 mm
NG 100	Laminar flow	d = 10 mm
NG60 H40	Laminar flow	d = 10 mm

Results with air - Isothermal flow		
Air	Laminar/ turbulent flow	d = 7 mm
Air	Laminar/ turbulent flow	d = 10 mm
Air	Laminar/ turbulent flow	d = 14 mm

Figure 2.5: Approach taken on PIV analysis.

A diameter of 10mm was chosen for the first phase of the analysis together with a Reynolds number of 500 and an equivalence ratio ϕ equal to 1 for the combustible mixtures NG 100 and NG60 H40.

In the second phase, using air as the studied fluid, three (3) diameters were used with eight (8) Reynolds numbers for each, accounting for a total of twenty four (24) PIV acquisitions performed in the second phase.

At the beginning of all acquisitions a calibration of the system was carried out using graph paper with 1mm subdivisions positioned in the diameter of the tube perpendicular to the camera. Two points at a distance of 10mm of each other were selected in DynamicStudio which allowed for the calibration of the software as well as for the calculation of the resolution (res) [pix/m] to use in the estimation of time interval between frames, Δt:

$$\Delta t < \min\left(\frac{[\mathrm{IA}_x, \mathrm{IA}_y] \times (1 - [o_{\mathrm{IA},x}, o_{\mathrm{IA},y}])}{[V_x, V_y] \times \mathrm{res}}\right) \tag{2.10}$$

with IA = [16,32] pix being the interrogation area defined and fixed for all acquisitions, o_{IA}= 75% the overlap between interrogation areas also fixed, and [V_x,V_y] calculated using the maximum possible estimated value in the flow field. Assuming $\mathrm{V}_x \sim$ 0 in this specific flow field, the maximum V_y can be estimated taking into account:

$$u = \frac{2Q}{\pi R^4}\left(R^2 - r^2\right) \tag{2.11}$$

$$\bar{u} = \frac{Q}{\pi R^2} \tag{2.12}$$

which leads to a maximum velocity in the yy directions of:

$$V_{y,max} = u(0) = \frac{2Q}{\pi R^2} = 2\bar{u} \tag{2.13}$$

Following the calibration process, the acquisition of images proceeded. A total of 200 pairs of frames for each acquisition were taken, using double frame mode, the minimum trigger rate possible of 15 Hz and the camera lens' aperture set to its maximum ($f/2.8$) which was meant to capture sufficient light from the tracer particles.

To start processing the frames in DynamicStudio, in order to end up with a unique vector field, it was fundamental to discard parts of the images acquired that could worsen the results accuracy by using "Black Out Masks" through all sets of frames. Subsequently, an analysis tool "Average Correlation" was applied, that was justified because the flow in study is statistically steady. For this tool, the values of interrogation area size and overlap mentioned above were used through all acquisitions.

After obtaining an unique vector field for a specific Reynolds number, the filter tool "UV Scatter Plot Range Validation" was applied to exclude vectors that don not fit within the expected range of values (such as vectors with negative vertical components). An example of the use of this tool is shown in Fig. 2.6, where the red arrows emphasise the vectors that don not make sense within the set.

The processed vector fields were exported to TecPlot 360 where precise lines of vectors were extracted

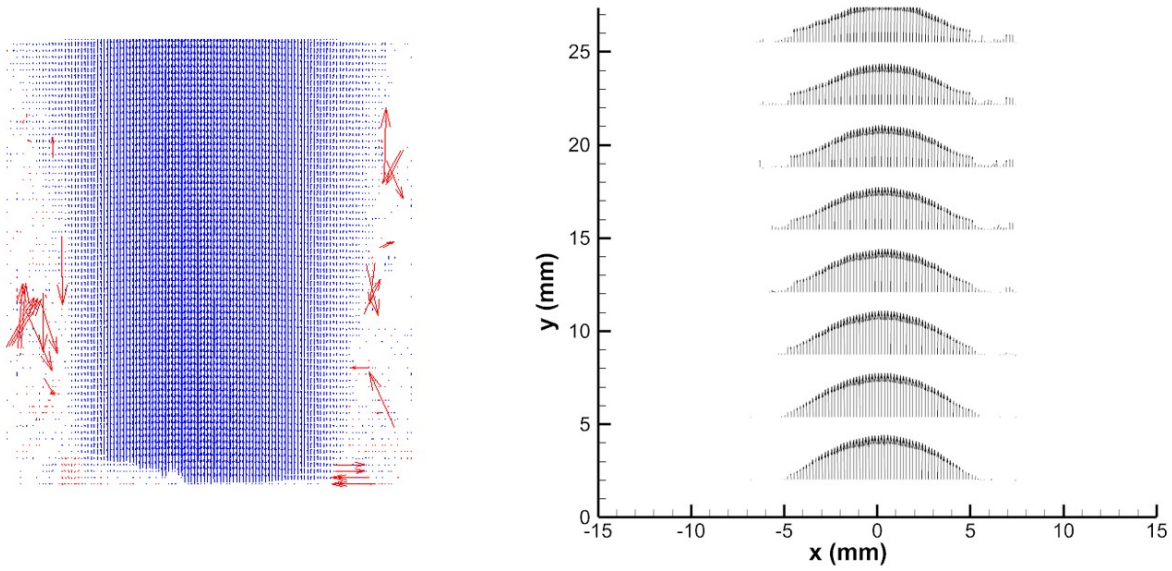

Figure 2.6: Post processing of a vector field using UV Scatter Plot Range Validation (left) and TecPlot processing (right)

as near as possible from the Burner's exit where the origin of the graph on the right of Fig. 2.6 is located.

After the extraction of the velocity profiles, each were manually processed to ensure the profiles complied with the no split boundary conditions that dictate the velocity to be zero at the walls. This was done by forcing $V_y = 0$ at $x = r$ and $x = -r$.

Chapter 3

Results

In this chapter it will be presented and analysed the results obtained through the stability experiments mentioned in the previous section 2.1.2 in order to understand the impacts of the enrichment of natural gas with hydrogen in its stability. This is here done using equivalence ratio *vs* Re plots, flashback and blowoff critical velocity gradients and also Glassman diagrams. Also a dimensional approach that is suggested in the literature is tested in the data obtained.

Furthermore, the results of particle image velocimetry tests on the flow are also presented and velocity profiles of different flows are analysed.

3.1 Influence of H_2 enrichment of Natural Gas on flashback and blowoff stability limits

For flame stability experiments, the six mixtures studied, range of mixture equivalence ratios, tube diameters and other operating conditions are represented in Table 3.1.

Table 3.1: Operational conditions used for flashback and blowoff stability experiments.

Hydrogen enrichment, xH_2[%]	0, 5, 10, 20, 30, 40
Equivalence ratio, ϕ	0.8, 0.9, 1.0, 1.1, 1.2, 1.3
Bunsen tube diameter [mm]	7, 10, 14
Cooling water flow rate [slpm]	0.2

The first results to analyse are the Reynolds numbers at which each mixture encounters instability, both flashback and blowoff.

In Fig. 3.1 the curves with points that achieved instability for the chosen significant mixtures with maximum (NG60 H40) and zero hydrogen content (NG100) are presented for the intermediate tube size of d = 10mm.

The symmetrical flashback curves with maximum around ϕ=1,05 and the increasing non-symmetrical blowoff curves are as expected when using premixed and homogenised fuel and oxidants. The increasing

blowoff curves are non-symmetrical in opposition to the flashback curves due to, for fuel-rich mixtures, an increase of the mass flow rate causing a decrease in the equivalence ratio which approaches stoichiometry due to the dilution with ambient air.

When analysing the curves taking into account its mixtures, it is directly observable that the mixture with higher hydrogen content reached flashback instabilities relatively sooner than the natural gas, thus having a shorter range of stable flow velocities. In this case, for example, for stoichiometric conditions, the natural gas reached instability at Re=400, while adding a percentage of xH_2=40% caused the instability to happen at Re=830.

These differences are also expected as a consequence of the high laminar burning velocity of hydrogen, increasing the propensity of the occurrence of the flashback phenomena.

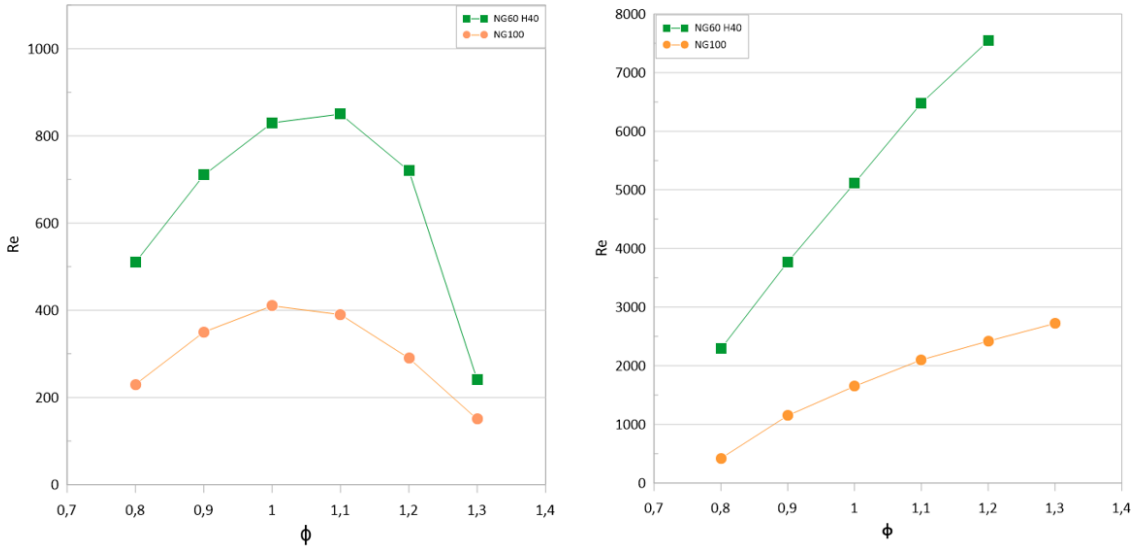

Figure 3.1: Flame flashback (left) and blowoff (right) stability tests for different mixtures (d=10mm).

On the contrary, the mixtures with higher hydrogen content only reached instability when increasing the flow rate much later than the mixtures without or with lower hydrogen content, as also observable in Fig. 3.1. For stoichiometric conditions, the flames left the Bunsen tube at Re=1650 and Re=5115.

All the other mixtures instability test data followed the same expected trends as the two examples shown and are plotted in Appendix A.

It is also interesting to note that in none of the flashback points the Reynolds number exceeds a value of 850. This means in all these cases the flow is laminar, while for most of the blowoff tests, specially for richer mixtures, the flows exhibited high turbulence reaching Reynolds numbers up to 7500. It is important to take into account that for the present case, flows are expected to present turbulent conditions for values higher than Re=2000.

The following step in the analysis is to take the approach using flashback and blowoff critical velocity gradients to later elaborate Glassman diagrams:

$$g_{\mathrm{F,B}} = \frac{8}{d} u_{av} = \frac{8\nu}{d^2}\mathrm{Re} \tag{3.1}$$

The results are shown in graphs $g_F = f(\phi)$ and $g_B = f(\phi)$ of Fig. 3.2 and compile the information from the three tube diameters resulting in an unique value for each fixed mixture and equivalence ratio ϕ.

Positive values of g_F and g_B as observed indicate that the average flow velocity at which flashback and blowoff occur increases with the tube's diameters. This is found in accordance with results found in the literature [17, 23, 24].

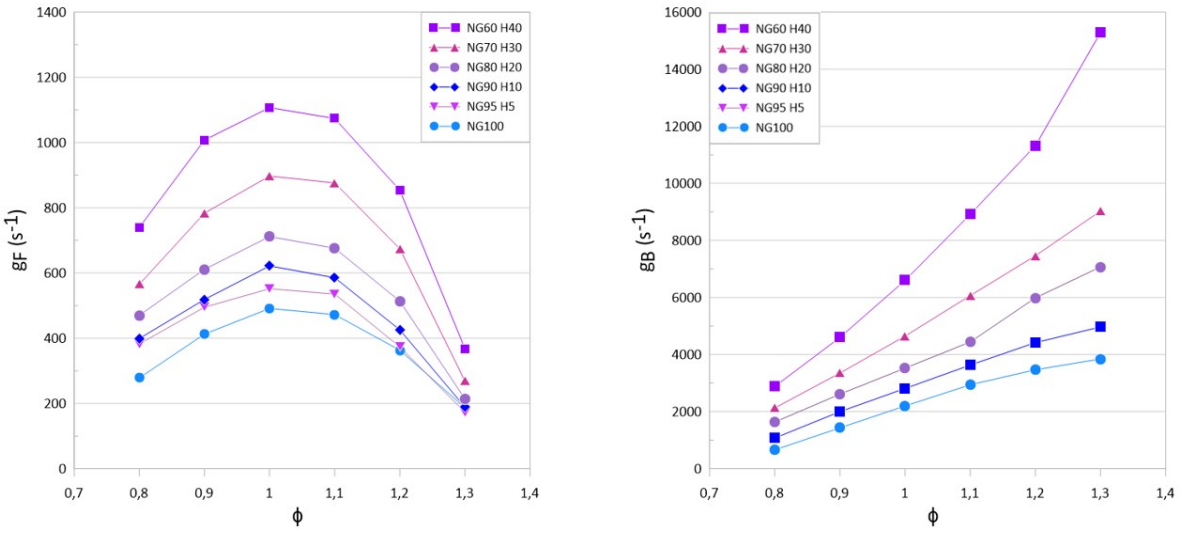

Figure 3.2: Flashback and blowoff critical velocity gradients for different mixtures of Natural Gas and Hydrogen

The impact on the curves when adding hydrogen is noticeable and pronounced, specially when 20% H_2 or more is used as a mixture. For the flashback curves on the left, critical velocity gradients range from value of 200 s^{-1} to 1100 s^{-1}, exhibiting the maximum values at about stoichiometric conditions for every mixture and the highest values overall for NG60 H40.

The blowoff limits show similar results, with critical velocity gradients ranging from 650 s^{-1} to about 15000 s^{-1}. A pronounced impact is found on the stability of the flames when adding more than 30% H_2 as the NG60 H30 shows a higher parabolic increase for richer mixtures. All the mixtures studies provided a maximum stability against blowoff for the richest equivalence ratio ϕ=1.3, as expected.

To obtain a parametric description of the variation of the gradients with hydrogen percentage xH_2 and equivalence ratio ϕ, the data presented on Fig. 3.2 on the left regarding the flashback gradients can be described accurately using second degree polynomial equations of the type:

$$g_F = a(\phi^2) + b(\phi) + c \tag{3.2}$$

In their turn, the polynomial constants a, b and c all vary linearly in such a way that can be described using xH_2 as an independent variable, resulting in:

$$a = a_1(xH_2) + a_2 \tag{3.3}$$

$$b = b_1(xH_2) + b_2 \tag{3.4}$$

$$c = c_1(xH_2) + c_2 \tag{3.5}$$

Calculating the constants a_1, a_2, b_1, b_2, c_1 and c_2 it is possible to obtain only one expression to describe the evolution of flashback gradient for values of hydrogen percentage and equivalence ratio others than the ones presented in this study, taking into account the validity of the data for the range $\phi = [0.8, 1.3]$ and $xH_2 = [0, 40]$:

$$g_F(xH_2, \phi) = (-127xH_2 - 3807)(\phi^2) + (257xH_2 + 7729)(\phi) + (-114xH_2 - 3461)[s^{-1}] \tag{3.6}$$

In the same way, in order to obtain a similar parametric description for the variation of the blowoff gradients with hydrogen percentage xH_2 and equivalence ratio ϕ, the data presented on Fig. 3.2 on the right can be described accurately using first degree polynomial equations, i.e, linear equations of the type:

$$g_B = d(\phi) + e \tag{3.7}$$

This suggested formulation seems to hold true for values of hydrogen percentage up to 30%, since from that point on the curve has a more strongly parabolic behaviour than linear as it can be noted in the NG60 H40 plot.

The polynomial constants d and e vary linearly in such a way that can be described using xH_2 as an independent variable, resulting in, as before:

$$d = d_1(xH_2) + d_2 \tag{3.8}$$

$$e = e_1(xH_2) + e_2 \tag{3.9}$$

Calculating the constants d_1, d_2, e_1 and e_2 it is obtained only one expression to describe the evolution of blowoff gradient for values of hydrogen percentage and equivalence ratio others than the ones presented in this study, taking into account the validity of the data for the range $\phi = [0.8, 1.3]$ and $xH_2 = [0, 30]$:

$$g_B(xH_2, \phi) = (249xH_2 + 6036)(\phi) + (-160xH_2 - 4050)[s^{-1}] \tag{3.10}$$

In the next section, the consequences of these results will be analysed with a practical application view such as domestic appliances or similar systems to Bunsen tubes.

3.2 Influence of H_2 enrichment of Natural Gas on the operation limits of a Bunsen Burner

When considering the design of Bunsen tubes and cooking stoves that use gaseous fuels, the importance of understanding stability limits becomes very clear. The maximum range of volumetric flow without experiencing stability concerns is desirable in the construction of a Bunsen burner.

With the goal of understanding the impact of H_2 enrichment in the operation of burners, the graphs $\bar{u}_v = f(d)$ shown in Fig. 3.3 and Fig. 3.4 were put together. In both figures the dashed area represents the region that has the greatest flow variability without stabilisation problems.

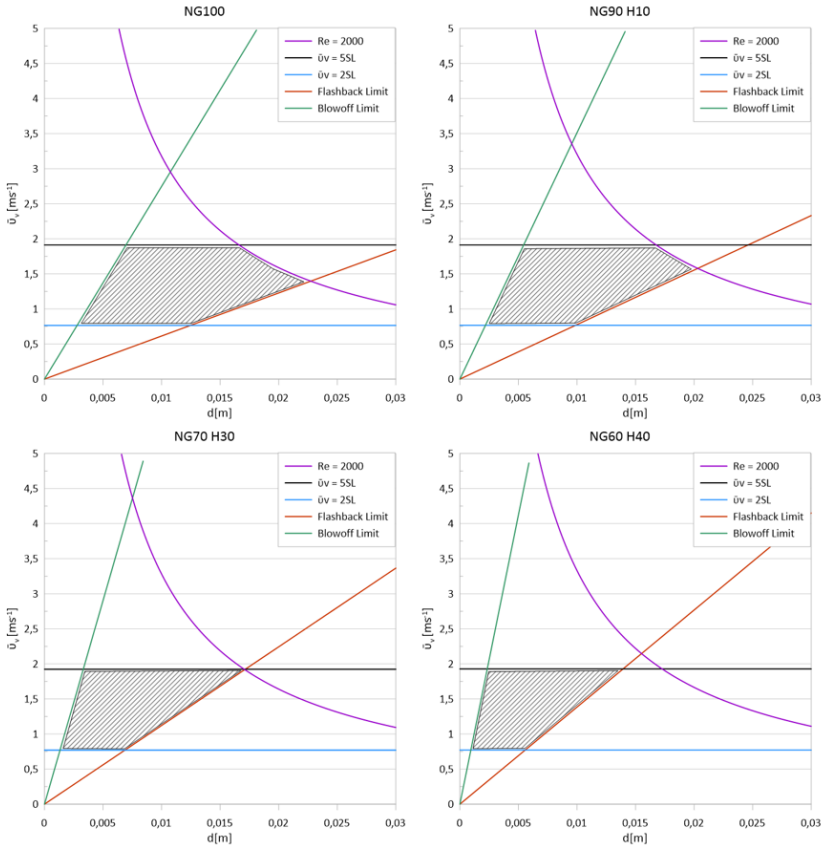

Figure 3.3: Operational area of Bunsen burners for different mixtures (ϕ=1)

To evaluate the laminar burning velocity S_L for the Glassman diagram the following equations were used.

Based on experimental data, the authors in [25] showed that the laminar burning velocities of natural gas/air and hydrogen/air, are well approximated (ϕ in the range 0.8-2.1) by Eqs. 3.11 and 3.12 :

$$S_{\mathrm{H_2}} = -1.11019 + 4.65167\phi - 1.44347\phi^2 + 0.04868\phi^3 \tag{3.11}$$

$$S_{\mathrm{NG}} = -0.0075 + \frac{0.1352}{4 \times (\phi - 1.04072)^2 + 0.34623} \tag{3.12}$$

To obtain the laminar burning velocity of for a HENG fuel with molar hydrogen percentage P_{H2} and

ϕ value (also in the range 0.8-2.1), it is suggested that Eq. 3.13, based on Eqs. 3.11 and 3.12, is used [15]:

$$S_{\mathrm{L}}\left(P_{\mathrm{H2}}\right)=\left(S_{\mathrm{NG}}+A_{\mathrm{HENG}}\Delta S_{\mathrm{L}}\left(\exp\left(\frac{P_{\mathrm{H2}}}{B_{\mathrm{HENG}}}\right)-1\right)\right)\mathrm{ms}^{-1} \tag{3.13}$$

where ΔS_{L} denotes the difference between S_{NG} and S_{H2}, and the constants A_{HENG} and B_{HENG} have values of 9.24330x10^{-3} and 21.30807, respectively.

The first figure mentioned is populated with the $\bar{u}_v = f(d)$ Glassman diagrams of four mixtures (NG100, NG90 H10, NG70 H30, NG60 H40) with increasing H_2 percentage and a fixed equivalence ratio of ϕ=1. This progression allows for a visualisation of the impacts of H_2 enrichment of natural gas on the stability region of burners while keeping the same air to fuel ratio.

In one hand, the range variation of admissible flows $\bar{u}_v$ observed in this case is negligible, since values of $\bar{u}_v = f(d)$ between 0.75 ms^{-1} and ~1.9 ms^{-1} offer the maximum range in all mixtures, in opposition to what appears to be the case in Fig. 3.4. On the other hand, and taking into consideration that the best burner diameter is the one that allows for a higher range of admissible flows, the differences in blowoff and flashback limits contribute to a displacement to smaller diameters. For the case of only natural gas (NG100) values of diameters between d = 7.5mm and d=12mm seem to provide the maximisation of the dashed area without stability issues. Furthermore, a decrease in this area is considerable in both the mixtures NG90 H10 and NG70 H30, as well as in the mixture with 40% H_2, in which the maximisation of the dashed stable area happens for diameters between d = 2mm and d = 6mm.

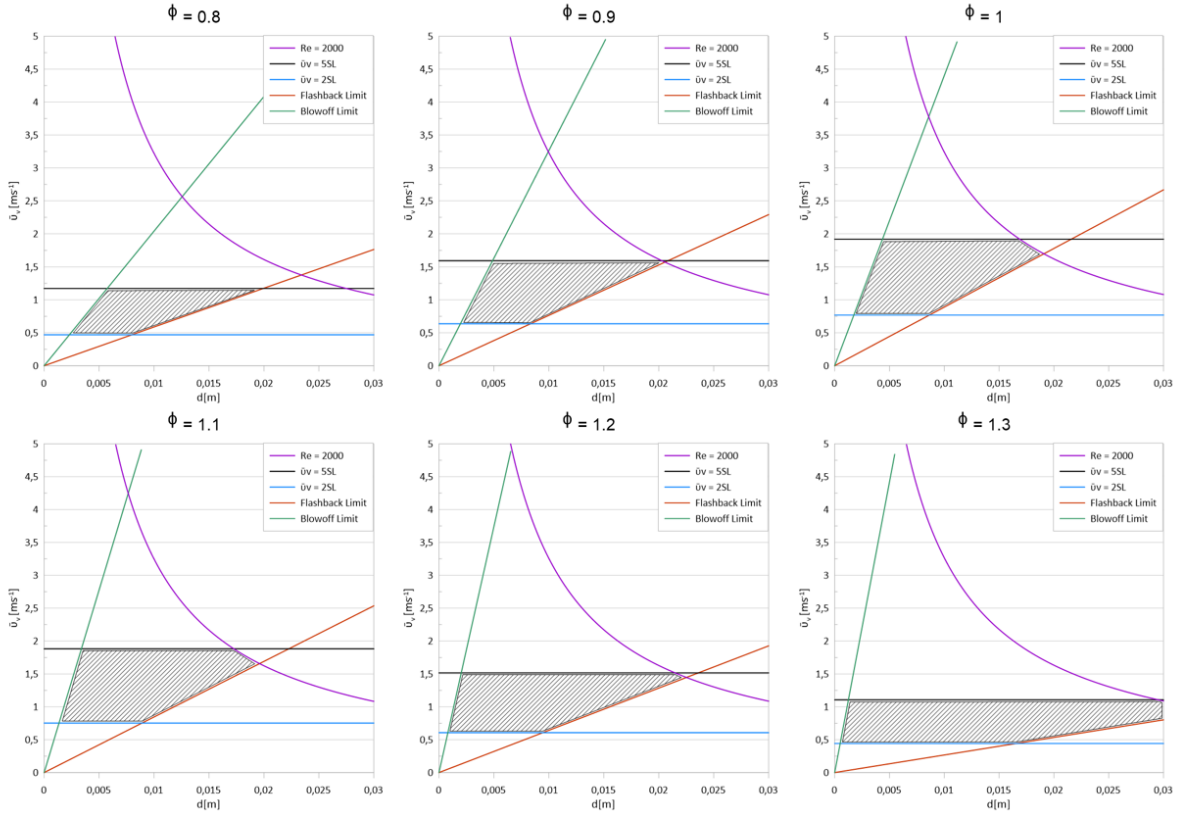

Figure 3.4: Operational area of Bunsen burners for different equivalence ratios (NG80 H20)

Figure 3.4 is populated with the $\bar{u}_v = f(d)$ Glassman diagrams of six mixtures. In this case of the same NG80 H20 mixture with variations of equivalence ratio between lean conditions ϕ=0.8 and rich conditions ϕ=1.3. Here, differences both in admissible flows and optimum diameters are noticeable. The equivalence ratio that provides a greater range of admissible flows is ϕ=1, while the leanest and richest compositions offer the smallest range. The former shows values of $\bar{u}_v = f(d)$ between 0.75 ms^{-1} and $\sim$1.9 ms^{-1} while the latter show a reduction of 47% to values of $\bar{u}_v = f(d)$ between 0.5 ms^{-1} and $\sim$1.1 ms^{-1}. This reduction is only of about 13.5% for ϕ=0.9 and only about 5% for ϕ=1.1.

Regarding optimum diameters to maximise the burner's stability, it is evident that the richest mixtures provide the biggest range of these six mixtures. For a equivalence ratio ϕ=1.3 the dashed area occupies the range between d $\sim$ 1mm and d $\sim$ 30mm, while in the leanest mixture of equivalence ratio ϕ=0.8 only values between d = 5mm and d = 7mm are advisable to be used in the design of Bunsen burners using NG80 H20 as a gaseous fuel.

The diagrams regarding the other mixtures studied are presented further in Appendix B and can be useful for analysing practical implementations and comparisons between mixtures and equivalence ratios.

3.3 Dimensional Analysis

The approach suggested by Putnam and Jensen [17] will be applied here and verified its applicability to the flashback data sets.

The authors suggested that the flashback propensity of a given fuel could be approximated using the relationship between the two "Peclet numbers":

$$Pe_J = \frac{1}{8K}(Pe_F)^2 \tag{3.14}$$

where K is a fuel-dependent constant and the final approximation holds when K/P_F is much less than one.

To test the theory proposed with the present flashback data, the square dependency of Eq. 3.14 and the variation of the constant K with different mixtures can be analysed.

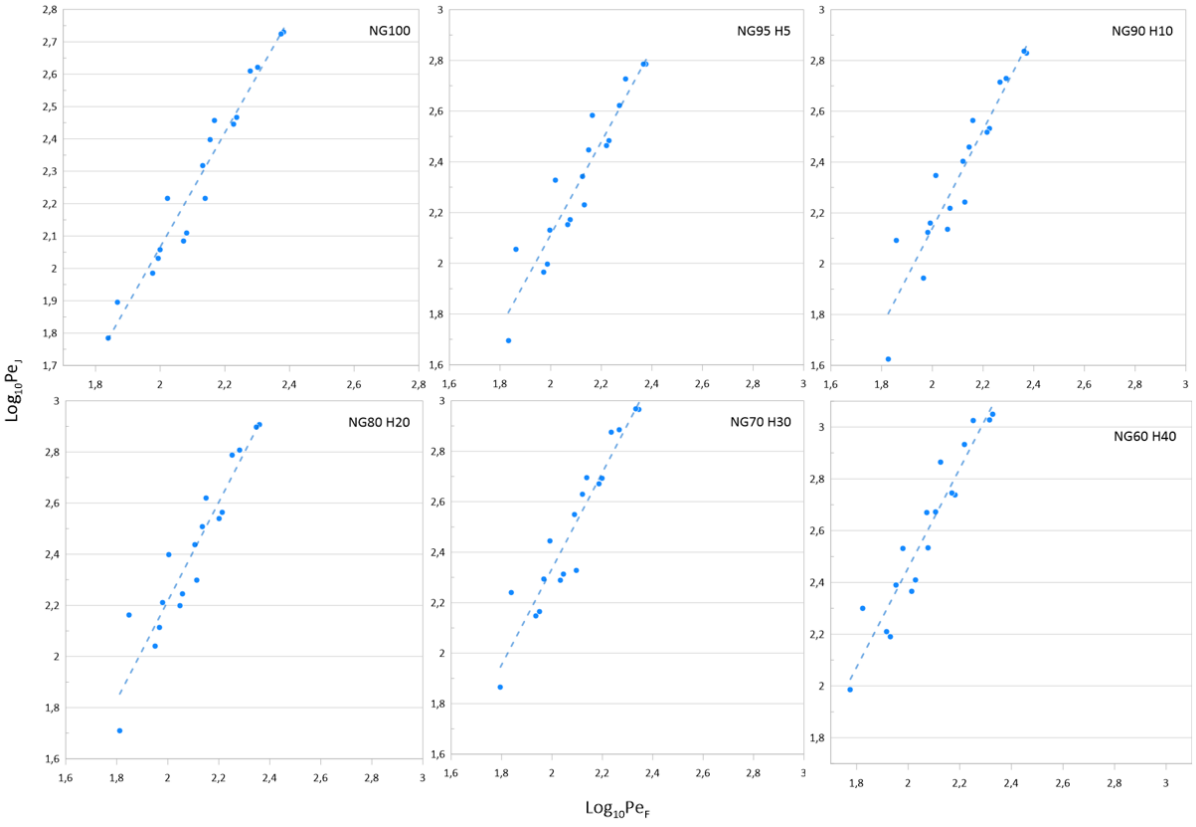

Figure 3.5: Scatter plots and respective linear regressions of logarithmic Peclet numbers for different mixtures

Applying logarithms to Eq. 3.14 one obtains:

$$\log_{10}(\mathrm{Pe_J}) = \log_{10}(1/8\mathrm{K}) + 2\log_{10}(\mathrm{Pe_F}) \tag{3.15}$$

It is now possible to plot this equation applied to the data collected for flashback instabilities and obtain a scatter plot. This scatter plot may follow a linear trend line of the form:

$$\log_{10}(\mathrm{Pe_J}) = b + a\log_{10}(\mathrm{Pe_F}) \tag{3.16}$$

in which the constant "a" will be taken as the slope of the linear polynomial and will be compared to the square dependency suggested in theory, and the constant "b" will be taken as the value of the linear polynomial in xx=0 and will result in the constant "K" by calculating : $K = \left(10^{-b}\right)/8$.

In Fig. 3.5 the six scatter plots with respective linear trend lines are shown. It is important to note that these linear trends were found to only appear when the data was analysed individually by mixture and did not appear when the data was analysed as a unique set. This might be a suggestion that the constants in analysis are, in fact, fuel-dependent.

In Table 3.2 the results of the linear regressions taken from the graphs above are broken down. The constants "a", "b", "K" and the coefficient of determination R^2 are brought forward.

Table 3.2: Linear polynomial regressions constants and coefficient of determination of graphs in Fig. 3.5

Mixture	**a**	**b**	**K**	**R^2**
NG100	1.7678	-1.4697	3.68	0.9526
NG95 H5	1.832	-1.5515	4.45	0.8914
NG90 H10	1.9319	-1.7242	6.62	0.8903
NG80 H20	1.9341	-1.6511	5.59	0.8952
NG70 H30	1.9054	-1.4761	3.74	0.9047
NG60 H40	1.9194	-1.3827	3.01	0.9095

The high values (around ∼0.9) of the coefficient of determination R^2 shows that the linear polynomial is in fact a good model to describe the present data and provide sufficient reliability to the following analysis.

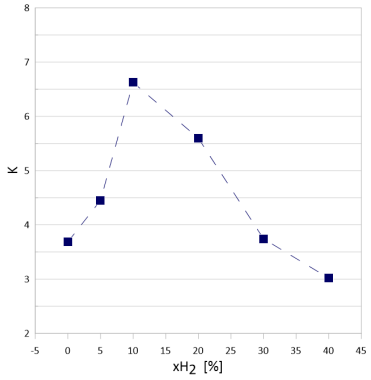

Figure 3.6: Variation of the constant K with change in hydrogen molar percentage in a HENG mixture

The slope "a" is found to be in the range of values between 1.7678 and 1.9341, with an average of 1.88. These are in average only 5.9% smaller than the suggested a=2 in theory, and only the mixture NG100 exhibits a slightly bigger deviation than would be wished.

In order to assess the impact the variation in the constant K has on the onset of flashback, both Eq. 3.17 and the graph in Fig. 3.6 can be useful:

Equation 3.14 can be re-written to take the form:

$$u_{\mathrm{av}} = \frac{{S_{\mathrm{L}}}^2 d_{\mathrm{port}}}{8K\alpha} \tag{3.17}$$

which allows the onset of flashback to be predicted across a range of u_{av} values.

It is a consequence of these that increasing the magnitude of K results in a decrease in the value of u_{av} for a given S_{L}, thereby lowering the susceptibility of the system to flashback. Taking this into consideration, and the values of K obtained, the mixture NG90 H10 would be the least susceptible to flashback while the mixture NG60 H40 would be the most susceptible to flashback, with K values of 6.62 and 3.01, respectively.

3.4 Velocity profiles and flow field - PIV

As described in the PIV methodologies Section 2.2.2, a two phase approach was taken in these experiments to obtain the velocity profiles at the Bunsen tubes exits.

First phase

The first phase had the goal of comparing, in isothermal conditions (no flame), the velocity profiles obtained when the studied mixture was pure air with the velocity profiles obtained from experiments using only CH_4 (NG 100) and the natural gas mixture with the highest xH_2 (NG60 H40). For this comparison to be valid, all the other variables were kept fixed such as the Reynolds number and tube diameter.

Table 3.3: Detailed approach and conditions under which phase one of PIV analysis was performed

	Mixture	**Reynolds Number**	**Equivalence Ratio**
	Air	500	-
1st Phase	**NG 100**	500	1
(d=10 mm)	**NG60 H40**	500	1

For this purpose, the three mixtures mentioned were tested in the 10mm diameter Bunsen tube, a Reynolds number of Re = 500 (providing laminar flow test conditions) and an equivalence ratio of $\phi = 1$ for the two combustible mixtures, NG100 and NG60 H40.

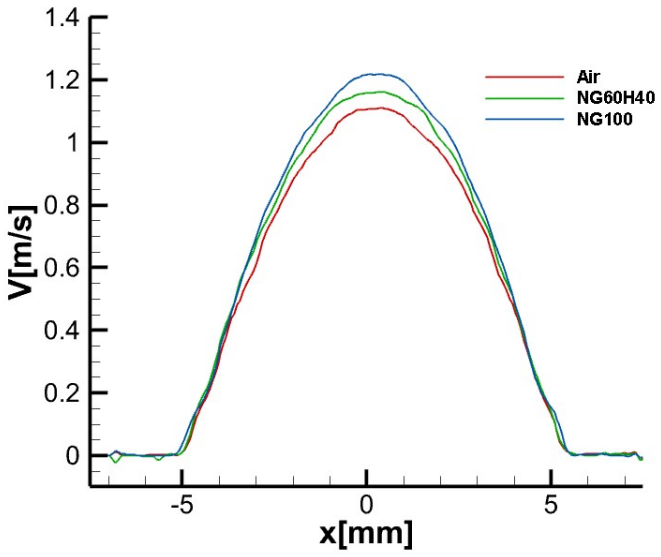

Figure 3.7: Velocity profiles at the end of Bunsen tubes for Re=500 and d=10mm for different mixtures

In Fig. 3.7 the plots of the three different velocity profiles obtained are presented in the form of a $V = f(x)[m/s]$ where x represents the distance between 0 and R or $-R$ millimetres from the axis of the tube. The three profiles have a parabolic shape and it can be observed some velocity difference in the

vicinity of $x = 0mm$ which can be explained by the different specific masses of the three mixtures and this being the region with the highest velocities, making these differences more impact-full. However, since the approach taken is intended to verify the usability of critical velocity gradients

$$g_{\mathrm{F,B}} \equiv -\lim_{r \to R}(dV/dx)$$

the differences in the centerline can be disregarded and the focus be put in the $\lim_{r\to R}(dV/dx)$. In this region, the three profiles actually overlap almost completely as can be seen as the limits $\lim_{r\to -5}(dV/dx)$ and $\lim_{r\to 5}(dV/dx)$ are the same in the plots shown.

Still in the first phase of the PIV experiments, the flow field streamlines were taken and analysed, also in isothermal conditions. The results are presented in Fig. 3.8 and show the streamlines for a flow of Air, Re = 500 and Bunsen tube diameter d = 10mm.

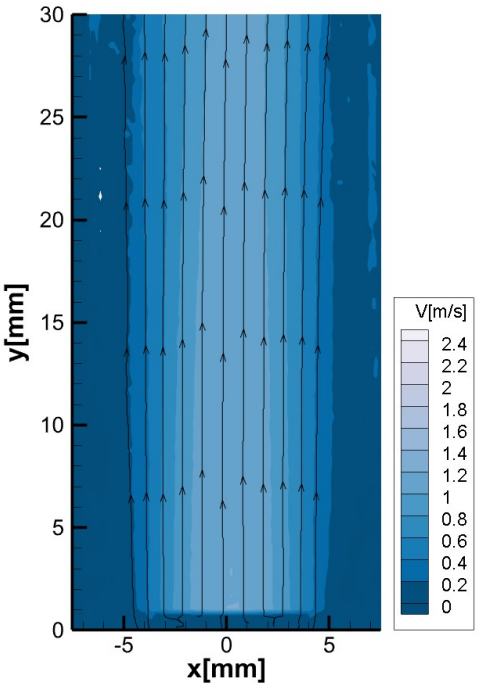

Figure 3.8: Flow field streamlines for Air, Re = 500 and d = 10mm

In the following subsection, some velocity profiles resulting from the second phase will be presented and analysed, taking into consideration that the first phase showed that Air could be used as a substitute for isothermal mixtures of natural gas and hydrogen when studying critical velocity gradients.

Second phase

The second phase of the PIV experiments had the goal of extracting the real velocity profiles of flows with Reynolds numbers that were significant to the study and comparing them with the expected theoretical velocity profiles for a Poiseuille flow.

Using air as the studied fluid, three (3) diameters were used with eight (8) Reynolds numbers for each diameter, accounting for a total of twenty four (24) PIV acquisitions performed in this phase. These conditions are detailed in Table 3.4.

Table 3.4: Detailed approach and conditions under which phase two of PIV analysis was performed

	Tube diameter	**Flashback Region**	**Blowoff Region**
	7 mm	Re = 100, 200, 300, 400	1000, 1500, 2000, 2500
2nd Phase	**10 mm**	Re = 400, 500, 600, 800	1500, 2500, 3500, 4500
(Air)	**14 mm**	Re = 500, 650, 780, 900	1350, 1850, 2230, 2500

Below in Fig. 3.9, nine velocity profiles are presented that were chosen to be representative of the results obtained and the most clear to analyse, as some results offered a poorer quality velocity profiles. This means, for example, presence of non-symmetrical velocity profiles, specially in experiments with higher Reynolds numbers where stronger turbulence was expected to be observed.

With the above mentioned, the tests with Reynolds numbers 100, 1000 and 2000 were chosen for d = 7mm; 500, 1500 and 3500 for d = 10mm and 500, 1350 and 2230 for d = 14mm. In each plot the black dots represent the velocity distribution of the stream of air at the orifice of the Bunsen measured experimentally and the black lines represents the calculated velocity distribution.

Analysing the smallest diameter of 7mm, all the velocity profiles measured experimentally obtained very close results to the calculated velocity distribution, exhibiting a parabolic shape, even when Re = 2000 was reached and turbulent region was attained.

When the tube in study had the diameter of 10mm, both Re = 500 and Re = 1500 velocity distribution profiles appear to follow the Poiseuille flow profile very close. However, in the third profile presented, as in some cases in the biggest tube, the velocity profiles did not approximate as well to the calculated velocity distribution and a "flattened" velocity profile was observed, with a non parabolic shape to it. This is the case of Re = 3500 presented, in which very turbulent conditions were observed.

Lastly, for the largest tube with a diameter of 14mm, the velocity distributions only overlap sufficiently the calculated velocity distribution up to Re = 1000. As can be seen by the 2 highest Reynolds shown here, Re = 1350 and Re = 2230, the profiles get more and more "flattened" as the air flow is increased. Nonetheless, the more laminar flows, here represented by Re = 500, still maintain a mostly parabolic shape that overlaps the Poiseuille flow profile plotted in the black line.

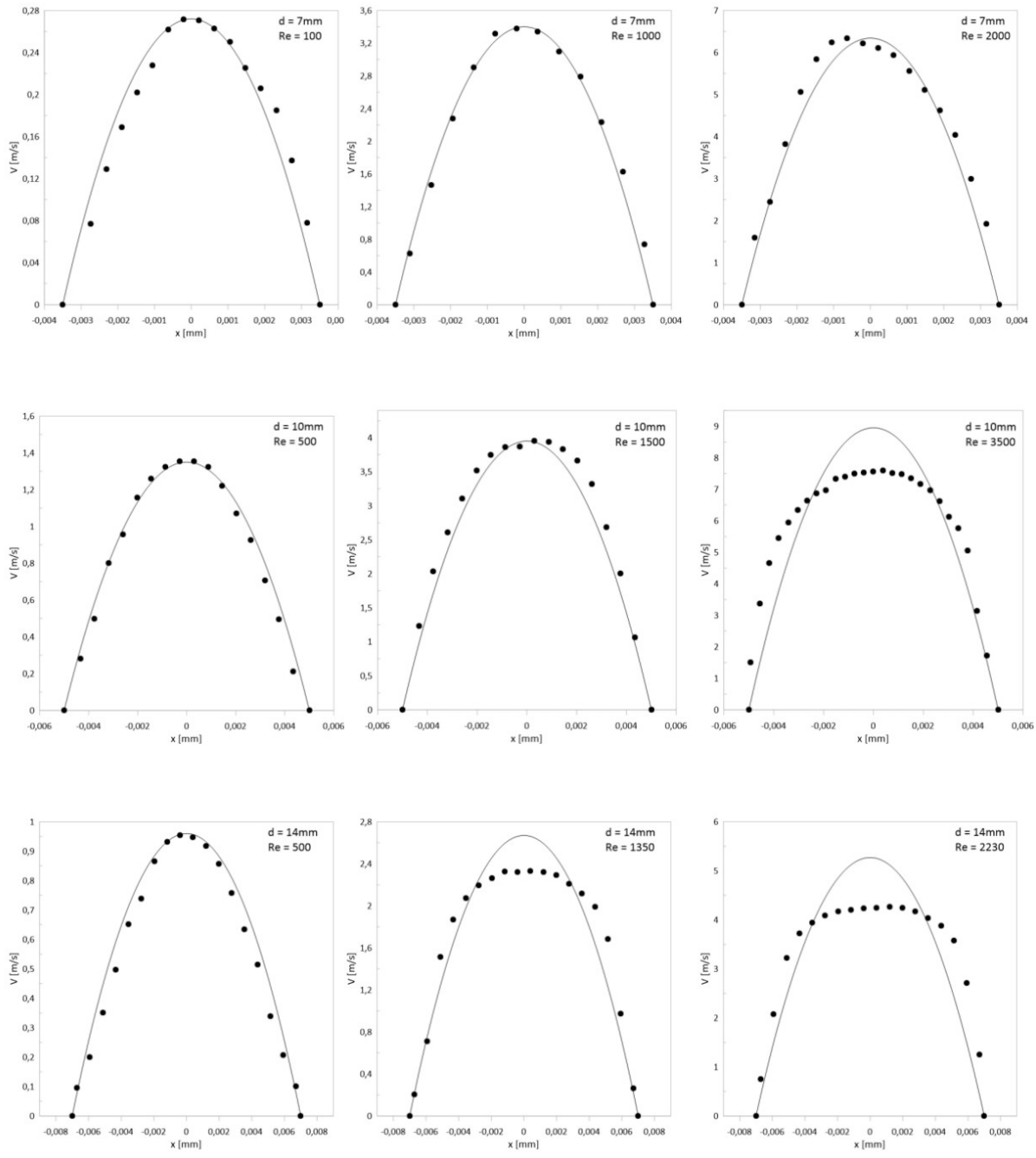

Figure 3.9: Velocity distribution in streams of air of different Reynolds numbers and tube diameters. Measured velocity and calculated velocity

Chapter 4

Conclusions

The main objective of this work was to assess the impacts of hydrogen enrichment of natural gas in fundamentals combustion aspects such as the flashback and blowoff phenomena in Bunsen Flames as a function of hydrogen enrichment. At the same time, use dimensional analysis tools to predict the onset of flame flashback and also apply particle image velocimetry techniques on the isothermal flow field to verify whether the underlying assumptions typically made on the study of critical velocity gradients were valid.

Six fuel mixtures were used, ranging from pure methane, NG100, to hydrogen-enriched natural gas with 40% volume percentage of H_2, NG60 H40. These were used in stability experiments using tubes with three different diameters, 7mm, 10mm and 14mm. Also, flame conditions for each mixture and tube were characterised by 6 different equivalence ratios, ranging from 0.8 to 1.3.

In the PIV experiments, also tubes with three different diameters were used (7mm, 10mm, 14mm) and a wide range of Reynolds numbers were chosen to mimic the conditions in which flame flashback and blowoff were observed in the stability analysis.

The main conclusions drawn from the work developed were:

The mixture with highest hydrogen content reached flashback instabilities relatively sooner than the natural gas. For stoichiometric conditions, d = 10mm, the natural gas reached instability at Re=400, while adding a percentage of xH_2=40% caused the instability to happen at Re=830.

The mixtures with higher hydrogen content only reached blowoff instability when increasing the flow rate much later than the mixtures without or with lower hydrogen content. For stoichiometric conditions, d = 10mm, the flames left the Bunsen tube at Re=1650 and Re=5115.

In none of the flashback tests the Reynolds number exceeded a value of 850. This means in all these cases the flow was laminar, while for most of the blowoff tests, specially for richer mixtures, the flows exhibited high turbulence reaching Reynolds numbers up to 7500.

The impact on the critical velocity gradients when adding hydrogen was noticeable and pronounced, specially when 20% H_2 or more was used. For the flashback curves critical velocity gradients ranged from value of 200 s^{-1} to 1100 s^{-1}, exhibiting the maximum values at about stoichiometric conditions for every mixture and the highest values overall for NG60 H40.

The blowoff limits showed similar results, with critical velocity gradients ranging from 650 s^{-1} to about 15000 s^{-1}. A pronounced impact is found on the stability of the flames when adding more than 30% H_2. All the mixtures studies provided a maximum stability against blowoff for the richest equivalence ratio ϕ=1.3.

Two equations describing the variation of the critical velocity gradients for natural gas with hydrogen percentage xH_2 and equivalence ratio ϕ were suggested as follows:

$$g_{\mathrm{F}}(xH_2, \phi) = (-127xH_2 - 3807)(\phi^2) + (257xH_2 + 7729)(\phi) + (-114xH_2 - 3461)[s^{-1}]$$

$$g_{\mathrm{B}}(xH_2, \phi) = (249xH_2 + 6036)(\phi) + (-160xH_2 - 4050)[s^{-1}]$$

Regarding the operation limits of a Bunsen burner, values of $\bar{u}_v = f(d)$ between 0.75 ms^{-1} and 1.9 ms^{-1} seemed to offer the maximum range in all stoichiometric mixtures. In the case of NG100 values of diameters between d = 7.5mm and d=12mm seem to provide the maximisation of the operational area without stability issues. Furthermore, a decrease in this area was considerable in both the mixtures NG90 H10 and NG70 H30, as well as in the mixture with 40% H_2, in which the maximisation of the operational stable area happens for diameters between d = 2mm and d = 6mm.

In one hand, the range variation of admissible flows $\bar{u}_v$ observed in this case is negligible, since values of $\bar{u}_v = f(d)$ between 0.75 ms^{-1} and 1.9 ms^{-1} offer the maximum range in all mixtures, in opposition to what appears to be the case in Fig. 3.4. On the other hand, and taking into consideration that the best burner diameter is the one that allows for a higher range of admissible flows, the differences in blowoff and flashback limits contribute to a displacement to smaller diameters. For the case of only natural gas (NG100) values of diameters between d = 7.5mm and d=12mm seem to provide the maximisation of the dashed area without stability issues. Moreover, a decrease in this area is considerable in both the mixtures NG90 H10 and NG70 H30, as well as in the mixture with 40% H_2, in which the maximisation of the dashed stable area happens for diameters between d = 2mm and d = 6mm.

When the mixture with highest hydrogen content accepted in Portugal taking into account the Wobbe Index was analysed, NG80H20, the equivalence ratio that provided a greater range of admissible flows was ϕ=1, while the leanest and richest compositions offered the smallest range. The former shows values of $\bar{u}_v = f(d)$ between 0.75 ms^{-1} and 1.9 ms^{-1} while the latter show a reduction of 47% to values of $\bar{u}_v = f(d)$ between 0.5 ms^{-1} and 1.1 ms^{-1}.

For a equivalence ratio ϕ=1.3 the dashed area occupied the range between d $\sim$ 1mm and d $\sim$ 30mm, while in the leanest mixture of equivalence ratio ϕ=0.8 only values between d = 5mm and d = 7mm are advisable to be used in the design of Bunsen burners using NG80 H20 as a gaseous fuel.

The dimensional analysis model showed good results when interpolating the results of flashback data, providing evidence that K is not in fact a constant, but varies significantly with different mixtures used. Taking the values of K obtained, the mixture NG90 H10 would be the least susceptible to flashback while the mixture NG60 H40 would be the most susceptible to flashback, with K values of 6.62 and 3.01, respectively.

The measured velocity profiles comparison against the calculated velocity profiles showed that the critical velocity gradients assumption of Poiseuille flow used typically can provide non realistic values when calculating blowoff critical velocity gradients, but for flashback velocity gradients typical Reynolds numbers, the measured velocity profiles overlap significantly with the calculated ones, making this a trustworthy assumption.

4.1 Future Work

As a continuation of the studies on this topic and specifically the deepening of the understanding of the influence of hydrogen enrichment on natural gas, with a view on practical applications and the importance of the subject in a near future, the following are suggestions for future work:

- Pursue a similar study to the one presented here, with smaller tube diameters (under d = 5mm), understanding the impacts that a scale-down would have on flame stability;
- Since this work only focused on HENG with hydrogen percentage up to 40%, it is imperative to continue increasing this percentage and try to mitigate the high impact on flashback propensity that that could bring;
- Another important aspect of studying HENG as a fuel is to make the transition from fundamental studies like this one and implement it in real-life systems such as home cooking stoves, water heating burners, and others, where flame interactions becomes another of the factors to take into account;
- As a final suggestion, applied specifically to work that would potentially be done in the same setup, would be to improve the water cooling sleeve that was designed, as to make it more robust.

Bibliography

[1] W. H. Organization. Health topics. URL `https://www.who.int/health-topics/`.

[2] D. G. de Energia e Geologia. Portugal key energy statistics, 2019.

[3] B. Pivovar, N. Rustagi, and S. Satyapal. Hydrogen at scale (h2@ scale): key to a clean, economic, and sustainable energy system. *Electrochemical Society Interface*, 27(1):47, 2018.

[4] E. Commission. A hydrogen strategy for a climate-neutral europe, July 2020.

[5] A. A. para a energia. Estratégia nacional para o higrogénio, Agosto 2020.

[6] S. R. Turns et al. *Introduction to combustion*, volume 287. McGraw-Hill Companies New York, NY, USA, 1996.

[7] I. Glassman, R. A. Yetter, and N. G. Glumac. *Combustion*. Academic press, 2014.

[8] G. Sivashinsky. Structure of bunsen flames. *The Journal of Chemical Physics*, 62(2):638–643, 1975.

[9] C. Dong, Q. Zhou, Q. Zhao, Y. Zhang, T. Xu, and S. Hui. Experimental study on the laminar flame speed of hydrogen/carbon monoxide/air mixtures. *Fuel*, 88(10):1858–1863, 2009.

[10] G. Andrews and D. Bradley. The burning velocity of methane-air mixtures. *Combustion and flame*, 19(2):275–288, 1972.

[11] P. Palies. Stabilization and dynamic of premixed swirling flames: Prevaporized, stratified, partially, and fully premixed regimes. 2020.

[12] B. Lewis and G. von Elbe. Stability and structure of burner flames. *The Journal of Chemical Physics*, 11(2):75–97, 1943.

[13] K. Altfeld and D. Pinchbeck. Admissible hydrogen concentrations in natural gas systems. *Gas Energy*, 2103(03):1–2, 2013.

[14] D. Haeseldonckx and W. D'haeseleer. The use of the natural-gas pipeline infrastructure for hydrogen transport in a changing market structure. *International Journal of Hydrogen Energy*, 32(10-11): 1381–1386, 2007.

[15] D. R. Jones, W. A. Al-Masry, and C. W. Dunnill. Hydrogen-enriched natural gas as a domestic fuel: an analysis based on flash-back and blow-off limits for domestic natural gas appliances within the uk. *Sustainable Energy & Fuels*, 2(4):710–723, 2018.

[16] T. Williams. European gas interchangeability. In *World Gas Conference*, 2009.

[17] A. A. Putnam and R. A. Jensen. Application of dimensionless numbers to flash-back and other combustion phenomena. In *Symposium on Combustion and Flame, and Explosion Phenomena*, volume 3, pages 89–98. Elsevier, 1948.

[18] Z. Duan, A. Kalantari, and V. McDonell. Parametric analysis of flashback propensity with various fuel compositions and burner materials. In *Turbo Expo: Power for Land, Sea, and Air*, volume 56697, page V04BT04A048. American Society of Mechanical Engineers, 2015.

[19] D. G. Goodwin, H. K. Moffat, and R. L. Speth. Cantera: An object-oriented software toolkit for chemical kinetics, thermodynamics, and transport processes, 2009.

[20] G. P. Smith, D. M. Golden, M. Frenklach, N. W. Moriarty, B. Eiteneer, M. Goldenberg, C. Bowman, R. K. Hanson, S. Song, W. C. Gardiner Jr, et al. Gri-mech version 3.0, 1999.

[21] M. Raffel, C. E. Willert, F. Scarano, C. J. Kähler, S. T. Wereley, and J. Kompenhans. *Particle image velocimetry: a practical guide*. Springer, 2018.

[22] S. DantecDynamicsA. Dynamicstudio user's guide. *Dantec Dynamics, Skovlunde*, 2013.

[23] D. Mishra. Experimental studies of flame stability limits of cng–air premixed flame. *Energy conversion and Management*, 48(4):1208–1211, 2007.

[24] P. Kurz. Some factors influencing stability limits of bunsen flames. *Combustion and Flame*, 1(2): 162–178, 1957.

[25] C. Dong, Q. Zhou, X. Zhang, Q. Zhao, T. Xu, et al. Experimental study on the laminar flame speed of hydrogen/natural gas/air mixtures. *Frontiers of Chemical Engineering in China*, 4(4):417–422, 2010.

Appendix A

Flame stability tests data

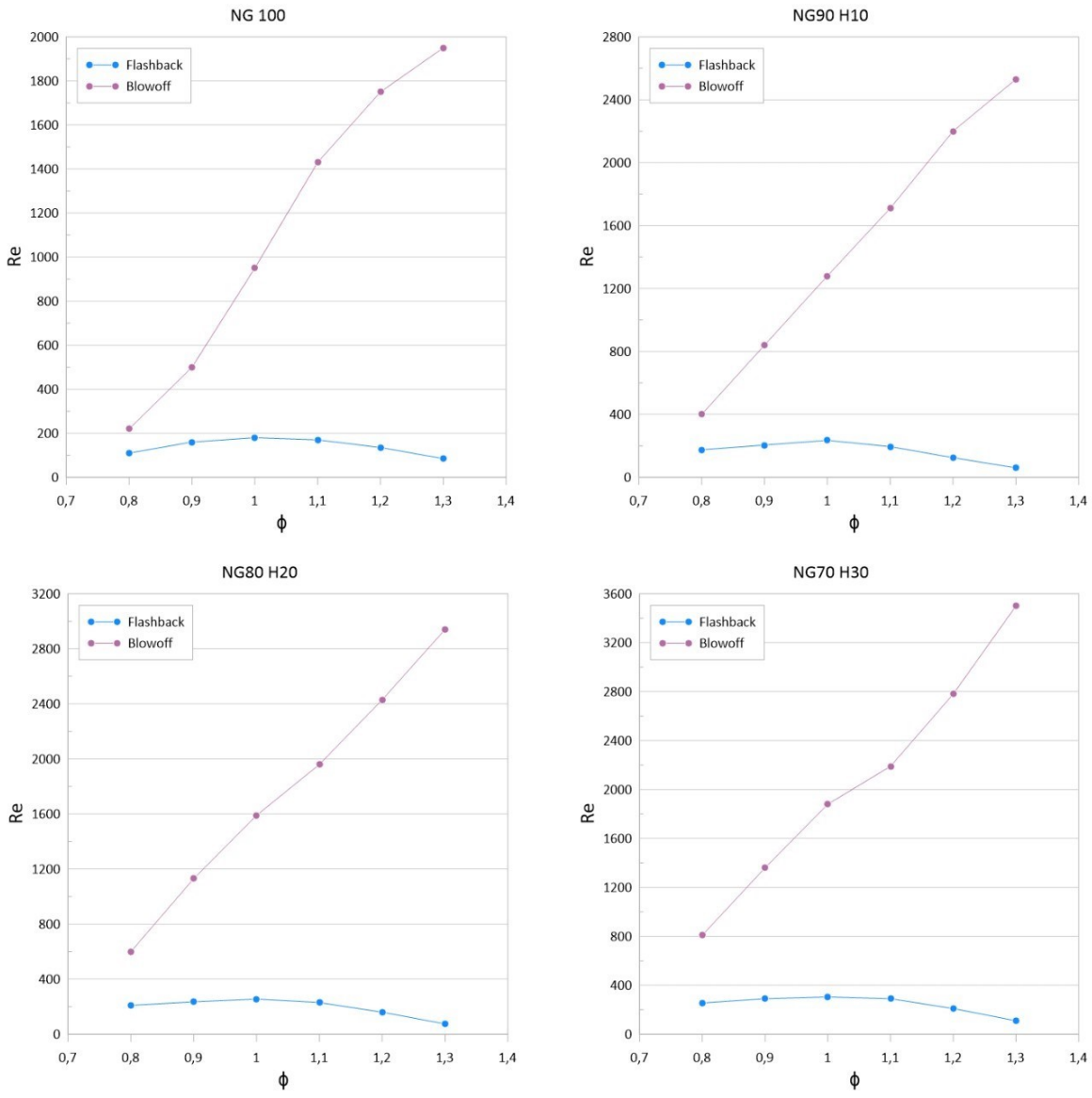

Figure A.1: Flashback and blowoff curves of 7 mm diameter Bunsen tube

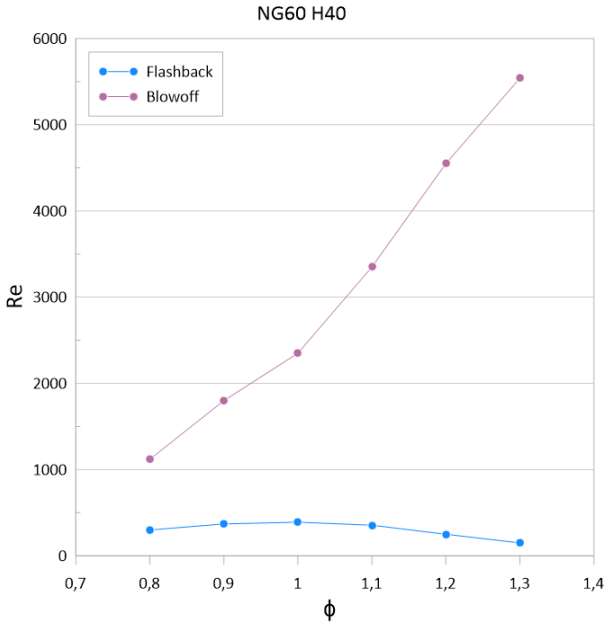

Figure A.2: Flashback and blowoff curves of 7 mm diameter Bunsen tube (cont.)

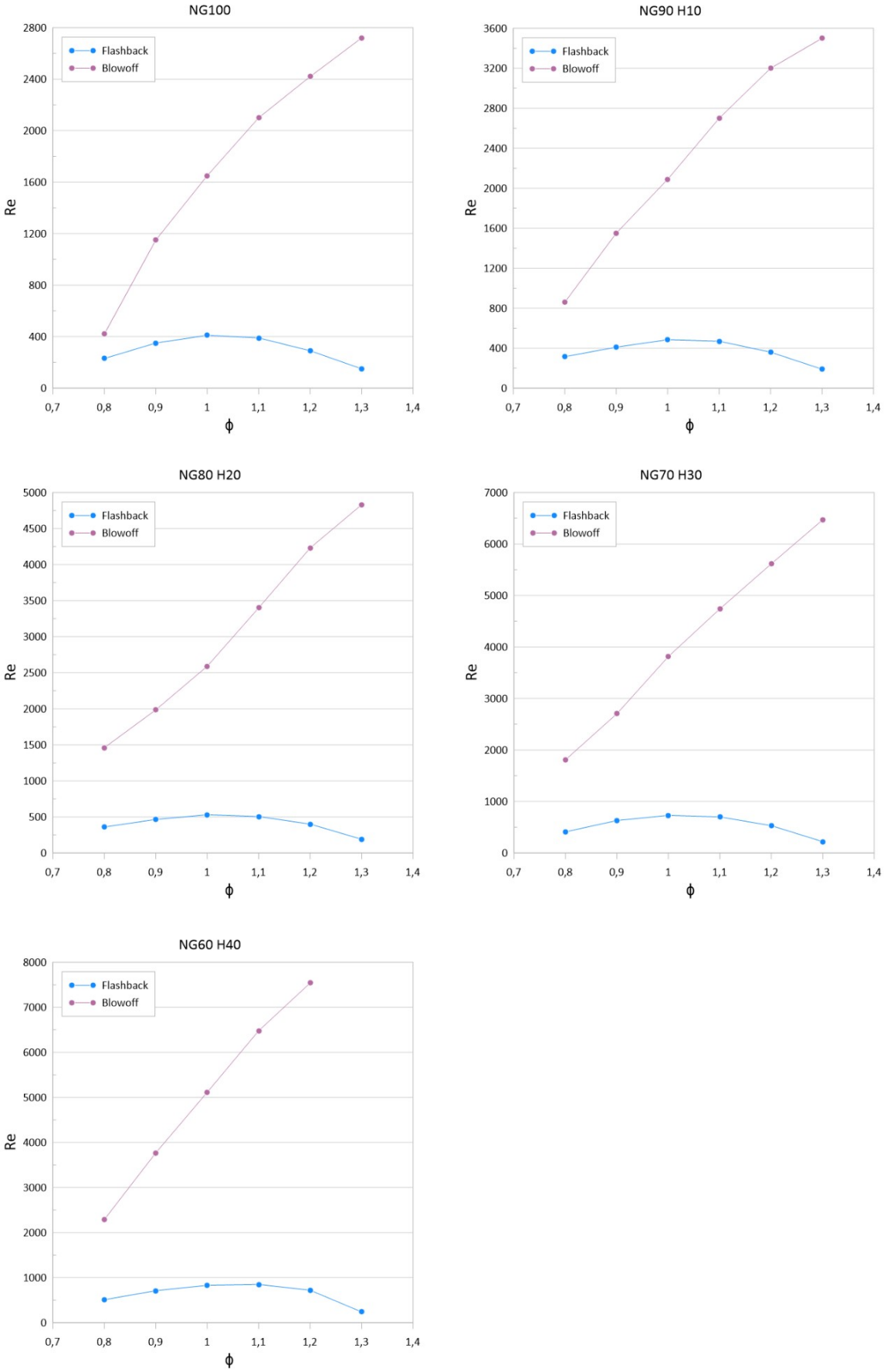

Figure A.3: Flashback and blowoff curves of 10 mm diameter Bunsen tube

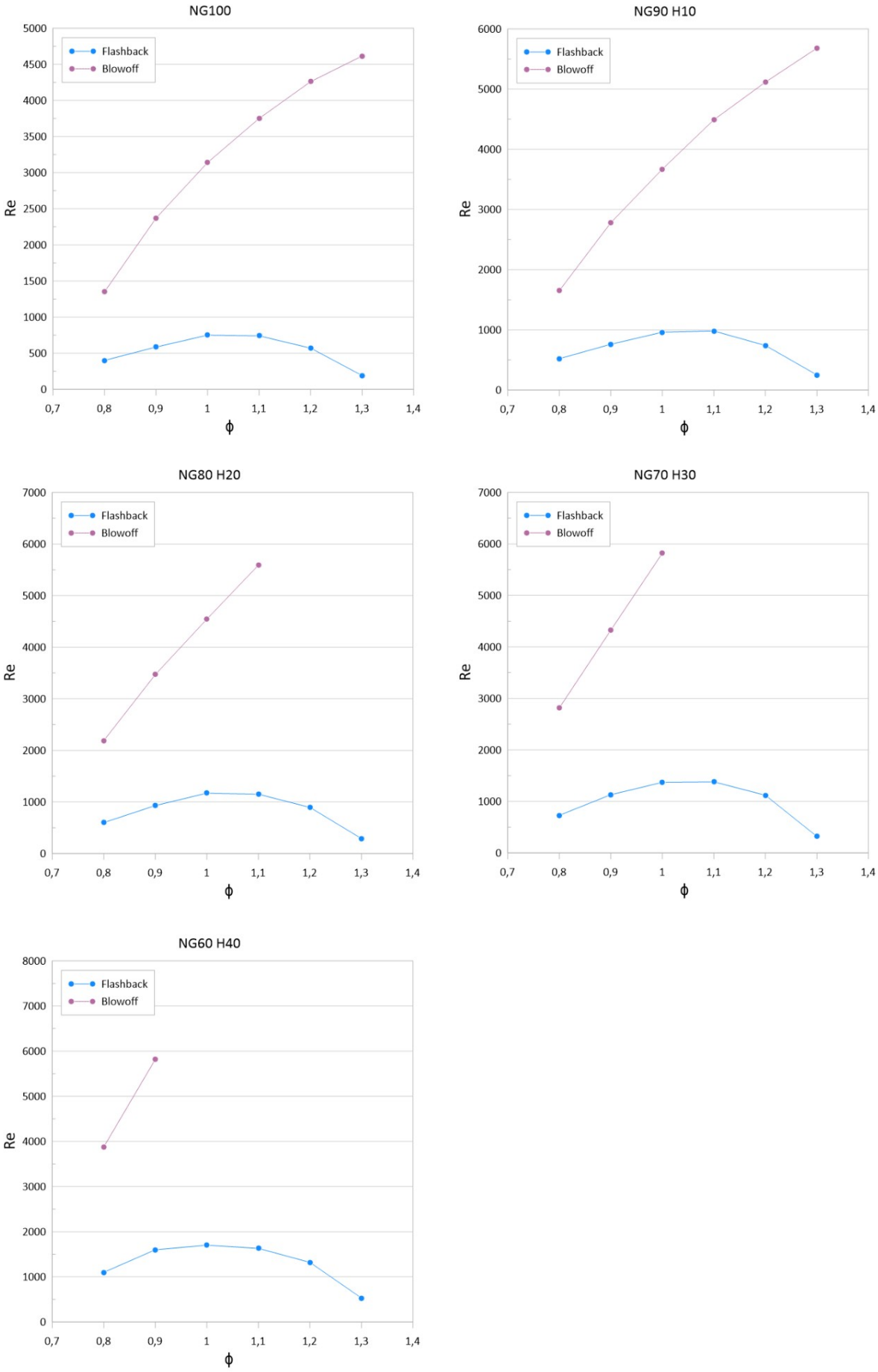

Figure A.4: Flashback and blowoff curves of 14 mm diameter Bunsen tube

Appendix B

Operational Area of Bunsen Burners - Glassman Diagrams

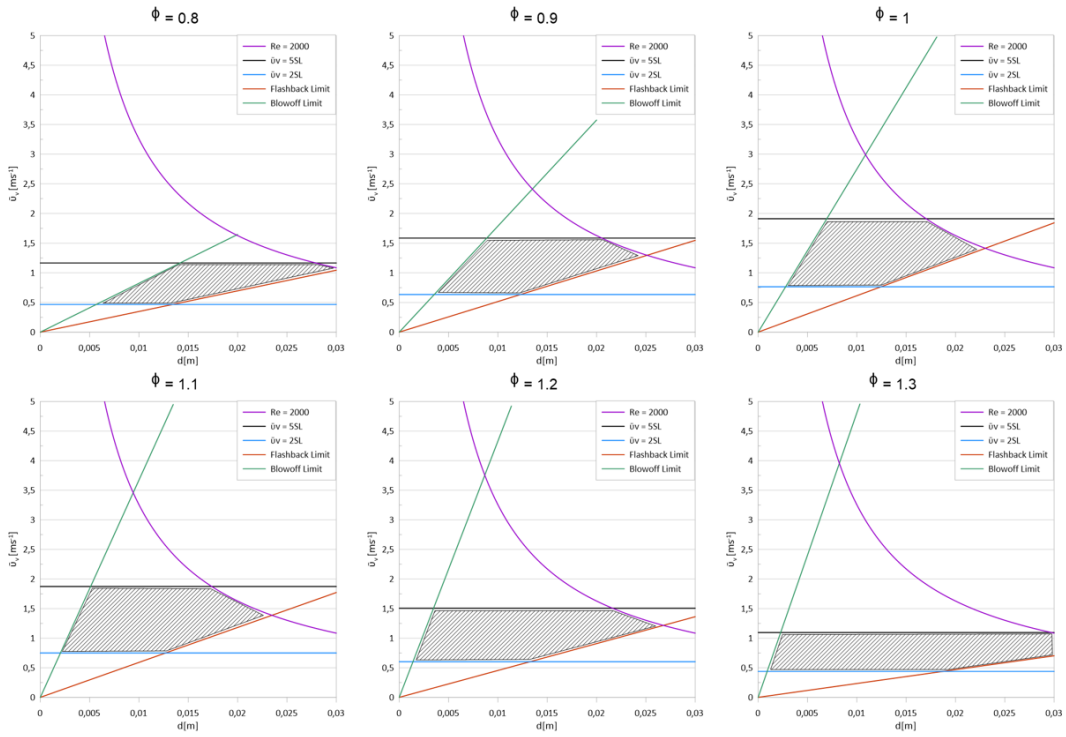

Figure B.1: Operational area of Bunsen burners for different equivalence ratios (NG100)

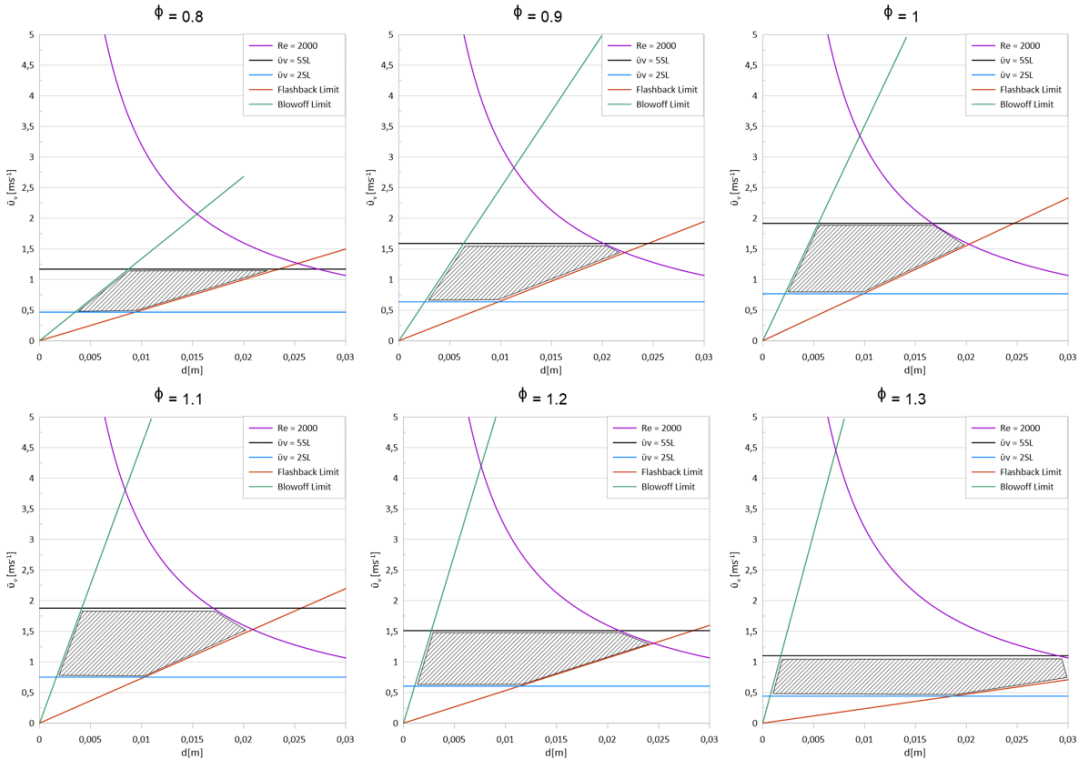

Figure B.2: Operational area of Bunsen burners for different equivalence ratios (NG90 H10)

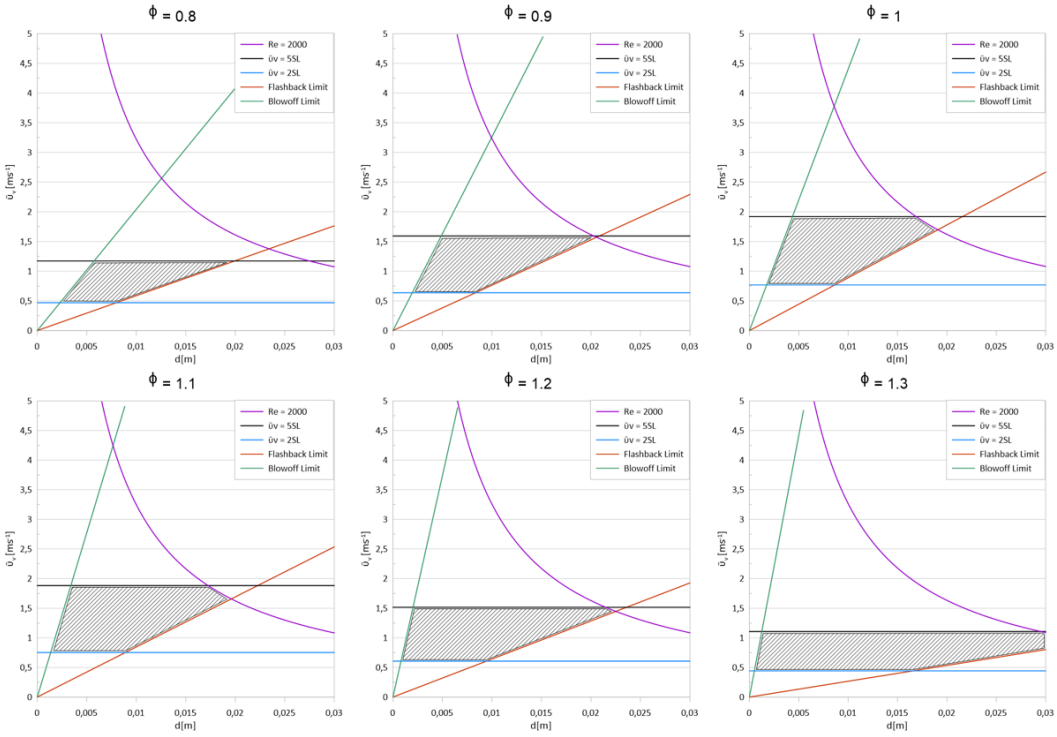

Figure B.3: Operational area of Bunsen burners for different equivalence ratios (NG80 H20)

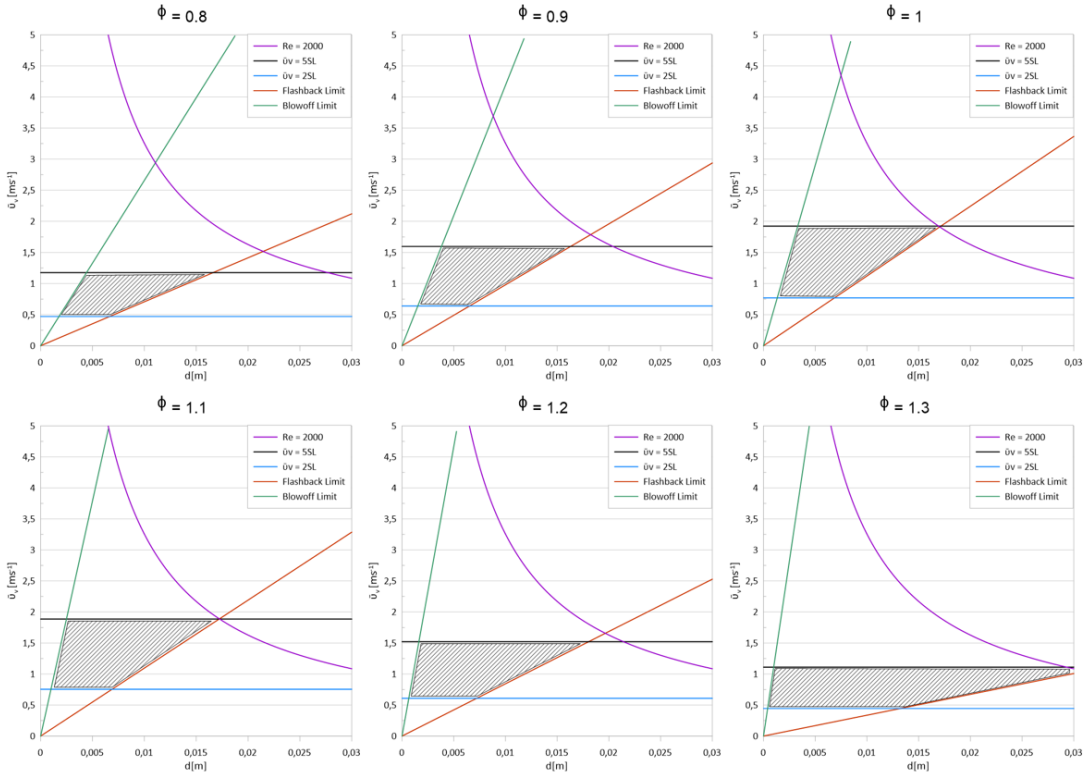

Figure B.4: Operational area of Bunsen burners for different equivalence ratios (NG70 H30)

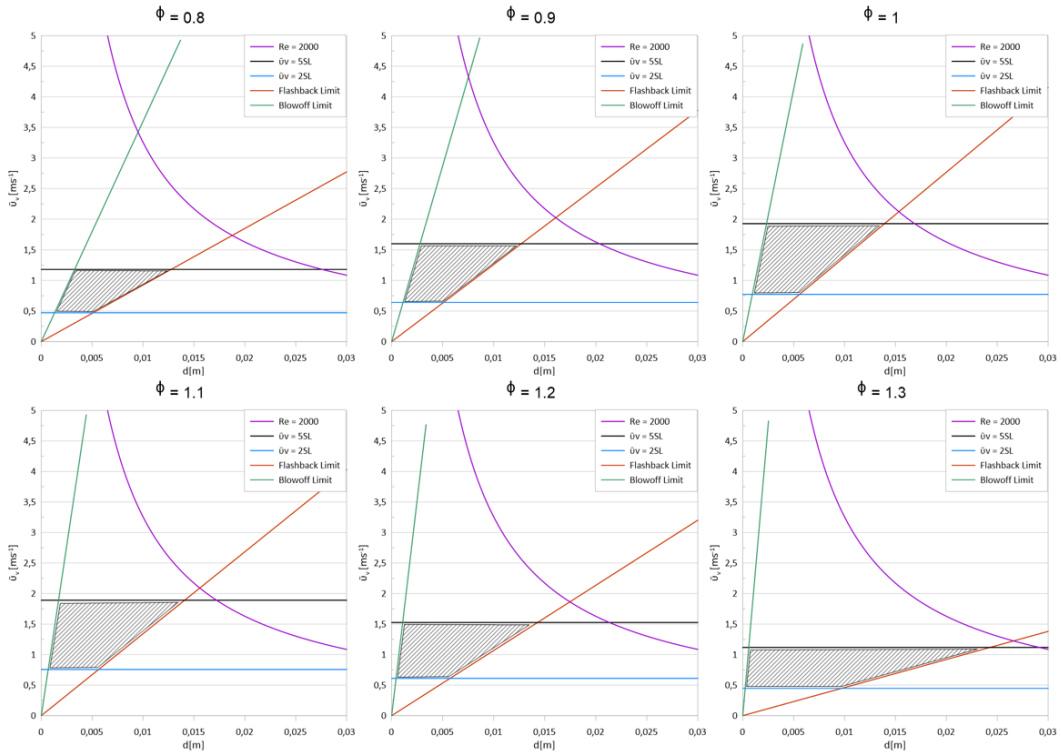

Figure B.5: Operational area of Bunsen burners for different equivalence ratios (NG60 H40)